

Land–Snow Data Assimilation Including a Moderately Coupled Initialization Method Applied to NWP

STANLEY G. BENJAMIN,^a TATIANA G. SMIRNOVA,^{b,a} ERIC P. JAMES,^{b,a} LIAO-FAN LIN,^{c,a} MING HU,^a
DAVID D. TURNER,^a AND SIWEI HE^{b,a}

^aNOAA/Global Systems Laboratory, Boulder, Colorado

^bCooperative Institute for Research in Environmental Sciences, University of Colorado Boulder, Boulder, Colorado

^cCooperative Institute for Research in Atmospheres, Colorado State University, Fort Collins, Colorado

(Manuscript received 18 October 2021, in final form 2 February 2022)

ABSTRACT: Initialization methods are needed for geophysical components of Earth system prediction models. These methods are needed from medium-range to decadal predictions and also for short-range Earth system forecasts in support of safety (e.g., severe weather), economic (e.g., energy), and other applications. Strongly coupled land–atmosphere data assimilation (SCDA), producing balanced initial conditions across the land–atmosphere components, has not yet been introduced to operational numerical weather prediction (NWP) systems. Most NWP systems have evolved separate data assimilation (DA) procedures for the atmosphere versus land/snow system components. This separated method has been classified as a weakly coupled DA system (WCDA). In the NOAA operational short-range weather models, a moderately coupled land–snow–atmosphere assimilation method (MCLDA) has been implemented, a step forward from WCDA toward SCDA. The atmosphere and land (including snow) variables are both updated within the DA using the same set of observations (aircraft, radiosonde, satellite radiances, surface, etc.). Using this assimilation method, land surface state variables have cycled continuously for 6 years since 2015 for the 3-km NOAA HRRR model and with CONUS cycling since 1997. Month-long experiments were conducted with and without MCLDA for both winter and summer seasons using the 13-km Rapid Refresh model with atmosphere (50 levels), soil (9 levels), and snow (up to 2 layers if present) on the same horizontal grid. Improvements were evident for 2-m temperature for all times of day out to 6–12 h for both seasons but stronger in winter. Better temperature forecasts were also shown in the 1000–900-hPa layer corresponding roughly to the boundary layer.

SIGNIFICANCE STATEMENT: Accuracy of weather models depends on accurate initial conditions for soil temperature and moisture as well as for the atmosphere itself. This paper describes a moderately coupled data assimilation method that modifies soil conditions based on forecast error corrections indicated by atmospheric observations. This method has been tested for a month-long period in summer and winter and shown to consistently improve short-range forecasts of 2-m temperature and moisture. This coupled data assimilation method is used already in NOAA operational short-range models to improve its prediction skill for clouds, convective storms, and general weather conditions.


KEYWORDS: Land surface; Boundary layer; Hydrometeorology; Snow cover; Soil moisture; Soil temperature; Surface fluxes; Surface observations; Numerical weather prediction/forecasting; Operational forecasting; Coupled models; Data assimilation; Land surface model

1. Introduction

Today's numerical weather prediction (NWP) models are, in fact, numerical Earth system weather prediction (NEWP) models (e.g., Benjamin et al. 2019) including internal prognostic treatment of land/vegetation, snow, ice, lakes, waves, and atmospheric composition. Representation of transfers of energy and moisture through these Earth system boundaries is an essential component of these prediction models. Lewis Richardson foresaw 100 years ago the importance of diabatic and viscous processes for successful atmospheric NWP, dedicating 40% of his book on them (Richardson 1922) and 10% of the book on processes related to surface, soil, and sea (Lynch

2006). Land surface models representing vertical transfers of heat and moisture to better represent surface fluxes were first introduced into climate models by the 1970s and 1980s (Randall et al. 2019). For weather-prediction models, initial slab models were later replaced by multilevel soil models (e.g., Ek et al. 2003; Smirnova et al. 1997).

With significant reservoirs of heat and moisture in the top few meters of depth in the soil, snow, and water, accurate specification of these conditions has been recognized as critical for NWP accuracy but difficult to accomplish (e.g., Koster et al. 2004). We assert that available observations, including atmospheric observations, should be used as effectively as possible to correct forecast errors in all Earth system components including near-surface soil–snow conditions. Here, we describe an effective one-way coupling from the atmospheric analysis increments to the land–snow state using approximate coupled correlations, a method we call a “moderately coupled” land data assimilation (MCLDA). MCLDA follows other efforts on land data assimilation, but it is

 Denotes content that is immediately available upon publication as open access.

Corresponding author: Stan Benjamin, stan.benjamin@noaa.gov

DOI: 10.1175/JHM-D-21-0198.1

For information regarding reuse of this content and general copyright information, consult the [AMS Copyright Policy \(www.ametsoc.org/PUBSReuseLicenses\)](https://www.ametsoc.org/PUBSReuseLicenses).

coupled within the three-dimensional atmospheric data assimilation technique with all atmospheric observations including screen-level measurements.

We describe details on the problem and possible approaches in section 2. Next in section 3, before describing a solution, we briefly describe an NWP system in which it is applied and tested: the NOAA regional 3-km High-Resolution Rapid Refresh (HRRR; Dowell et al. 2022, hereafter D22; James et al. 2022, hereafter J22) and its parent 13-km Rapid Refresh (RAP) modeling systems (Benjamin et al. 2016, hereafter B16). Section 4 provides a detailed description of the coupled data assimilation method itself, and section 5 describes the complementary snow-cover assimilation technique. Results from a set of experiments using the RAP model–assimilation system to test this method are presented in section 6, followed by conclusions in section 7.

2. Motivation: The problem and the opportunity

Daytime warm biases in 2-m temperature and dry biases in 2-m dewpoint forecasts have been evident in warm season over continental areas in hourly-updated operational weather models despite reduction in recent years (B16; Lee et al. 2019; Fovell and Gallagher 2020). This problem has a longer history: a warm daytime bias over continental areas in warm season has been singled out as an outstanding continuing issue for many climate and weather models (e.g., Klein et al. 2006; Morcrette et al. 2018; Ma et al. 2018). Koster et al. (2004) linked this problem to a soil moisture bias. Mitchell et al. (2004) stated that the main error sources in land state forecasts are errors in precipitation and shortwave radiation, eventually leading to biases in soil states, as suggested earlier by Viterbo and Beljaars (1995). As in the real world, land surface models (LSMs) are “reservoirs” of the days-/weeks-/months-long outcome from the modeled atmospheric processes, and as models, these LSMs collect a longer-term signal of potential biases in atmospheric forcing. Their evolving soil moisture and temperature fields are the “canaries in the coal mine,” collecting over time the effects of thermal/radiative and water-cycle errors from components of the atmospheric models and therefore, a possible early signal of the mean errors in the model representations of the atmospheric processes.

As precipitation analyses based on infrared and microwave satellite data became available (e.g., Xie and Arkin (1996, 1997) along with satellite-based cloud products, better atmospheric forcing variables enabled stand-alone “land data assimilation systems” (LDASs) to estimate updated values of soil moisture/temperature, a vast improvement over climatological soil moisture. A pioneering LDAS applied for North America (NLDAS) using prescribed atmospheric forcing including precipitation, temperature, wind, water vapor, and radiation (Mitchell et al. 2004) in a separate domain for the land. The current NOAA Global Land Data Assimilation System (GLDAS) was updated in March 2021 as part of GFSv16 to use an updated version of its land surface model (Noah LSM) with updated soil parameters (Xia et al. 2020, 2021). The U.S. GLDAS follows the design of the NOAA NLDAS (Mitchell et al. 2004) in its reliance on precipitation analyses. Satellite-based estimates of precipitation

have improved with increased availability of microwave data [e.g., TRMM (Tropical Rainfall Measuring Mission, mission over 1997–2015; Huffman et al. 2007) and its successor IMERG (Integrated Multi-satellite Retrievals for GPM; Huffman et al. 2019)].

Meanwhile, an initial coupled DA used screen-level observations of temperature and humidity to improve soil moisture (Mahfouf 1991), a technique still foundational for many centers to initialize land surface fields (e.g., Giard and Bazile 2000; Bélair and Boone 2020). Currently, operational NWP centers use some kind of LDAS approach to update land surface fields in their regional and global models. Table 1 provides a summary of some of these land-assimilation techniques including that presented in this paper. The LDAS approach is applied with coupled DA with 2-m temperatures and satellite observations for Canada (ECCC, Environment and Climate Change Canada; Bilodeau et al. 2016; Carrera et al. 2019), France (Météo-France; Giard and Bazile 2000), the U.K. Met Office (UKMO; Gomez et al. 2020), and the European Centre for Medium-Range Forecasts (ECMWF; de Rosnay et al. 2013, 2014; Muñoz-Sabater et al. 2019; Balsamo and Mahfouf 2020).

Using the nomenclature of Penny et al. (2017), the LDAS framework utilized in these offline NWP systems is a weakly coupled data assimilation (WCDA) framework with separate land surface and atmospheric data analyses. An assignment of the level of coupling by the Penny et al. nomenclature is included for some different coupled data assimilation frameworks in Table 1.

Satellite-based retrievals of soil moisture variables [e.g., Satellite Moisture and Ocean Salinity (SMOS), Soil Moisture Active Passive (SMAP), Advanced Scatterometer (ASCAT), Advanced Microwave Scanning Radiometer (AMSR)] have allowed further refinement on initial soil moisture accuracy through their assimilation in the NASA Land Information System (LIS; Kumar et al. 2008; Santanello et al. 2019) and in ECMWF, UKMO (Gomez et al. 2020), and Météo-France models (e.g., Mahfouf 2010; Draper et al. 2011; Dharssi et al. 2011; de Rosnay et al. 2014; Rodriguez-Fernandez et al. 2019). Assimilation of in situ soil moisture observations has been demonstrated by Lin and Pu (2020) in an experimental mode. However, the in situ probe measurements are often strongly limited in horizontal representativeness by local variations (often subkilometer scale) of soil type and recent convective-storm precipitation. Satellite retrievals of soil moisture are also limited by land surface heterogeneity and uncertainty in vertical depth of soil and vegetation contributions to satellite-based radiances. Carrera et al. (2019) summarize positive results in the Canadian NWP model with joint assimilation of screen-level temperature and moisture and satellite-based soil moisture estimates as improved for soil moisture (vs soil moisture observations) but also experienced increased biases for atmospheric screen-level humidity.

A frequent cycling approach has been implemented in the NOAA hourly updated RAP and HRRR models over North America. It was also used earlier from 1998 to 2012 with the NOAA Rapid Update Cycle model (RUC; Benjamin et al. 2010). In these models, accurate frequent observations related to precipitation and cloud conditions, including assimilation of radar reflectivity and lightning data (Weygandt et al. 2022;

TABLE 1. Coupling of land–snow and atmospheric data assimilation for different NWP systems.

Model	Atmosphere observations used for land		DA coupling	Variables updated	Soil obs used for land	Snow updating	References
	Atmosphere and land DA	Atmosphere					
NOAA GFS	Separate (LDAS)	None directly	Driven by precipitation analysis and atmospheric analyses	Soil moisture (SM), soil temp	None	USAF snow, not coupled, not updated from model forecast	Xia et al. (2020, 2021)
NASA LIS	LDAS, no atmospheric component	N/A	Coupled ensemble-based covariances	SM, soil temp	SMAP, SMOS	None	Kumar et al. (2008); Santanello et al. (2019) This paper
NOAA HRRR/RAP	Joint–MCLDA	All atmospheric obs including 2-m temp/humidity, raob, aircraft, radar, satellite radiance /cloud, etc.	Assumed simple covariance between full atmosphere and soil moisture/temp increments (MCLDA)	SM, soil temp, snow temp	None for soil	Cycled snow temp modified in MCLDA. Cycled SWE, snow depth. Updated sat-based snow cover (IMS).	Lin and Pu (2020)
NCAR ensemble	Cycling only, no coupled DA	—	Cycling only	None	None	None	Koukoulou et al. (2021)
ECMWF	WCDA (LDAS)	2-m temp, 2-m humidity	Point-wise simplified extended Kalman filter (SEKF)	SM, soil temp, snow	ASCAT, SMOS Tb	Updated snow cover (IMS), depth via separate 2D OI	Muñoz-Sabater et al. (2019)
ECCC–Canada	WCDA (LDAS)	2-m temp, 2-m humidity	EnKF	SM, soil temp, snow	SMAP, SMOS	Updated sat-based snow cover (IMS)	Carrera et al. (2019)
Météo-France	WCDA (LDAS)	2-m temp, 2-m humidity	OI scheme	SM, soil temp, snow	None	Sat-based snow cover (IMS)	Giard and Bazile (2000)
UKMO	WCDA (LDAS)	2-m temp, 2-m humidity	SEKF for both global and regional NWP	SM, soil temp, snow	ASCAT	Updated snow cover (IMS), snow depth, snow depth 2D OI-regional	Gomez et al. (2020)
Planned for NOAA UFS	Fully coupled, SCDA (likely)	All atmospheric obs, including 2-m T/Td, tropospheric obs, radar, satellite radar/cloud, etc.	Coupled ensemble-based covariances, soil/snow state is included into analyzed variables in SCDA	SM, soil temp, snow temp, snow water equivalent (SWE), snow depth	SMAP, SMOS, in situ, snow cover	Cycled, soil temp, SWE, snow depth/moisture and snow temp modified in SCDA	

B16; D22) and cloud observations (Benjamin et al. 2021), have allowed more accurate forward cycling (see Table 2) to improve the accuracy of the initial and short-term surface energy budgets. But even with these rapid high-resolution observations with land cycling, some drift in soil conditions can still occur due to systematic errors in precipitation or cloud–radiation forcing, especially in mountainous areas without complete radar data (including over much of the western United States). A recent example of ongoing cycling of land surface fields with 3-km modeling (similar to HRRR) and 3-hourly atmospheric DA (not coupled) was demonstrated by Koukoulou et al. (2021), showing closer agreement to NLDAS-2 soil fields than from the GFS.

Increased sophistication has been incorporated over the years within these WCDA/LDAS approaches. The LDAS schemes have evolved to more accurate ensemble-based schemes. As cited by Duerinckx et al. (2017), the advantage of the extended Kalman filter (EKF) technique over a simpler optimal interpolation (OI) approach is that it has a more generic formulation of the gain coefficients and thus can be extended toward new observation types (Mahfouf et al. 2009). However, weakly coupled land and atmospheric data assimilations without simultaneous increments may lead to sudden shocks to latent and sensible heat fluxes by abruptly changing the temperature and moisture vertical gradients across the atmosphere–surface interface. Mulholland et al. (2015) demonstrated and quantified this initialization shock from independent atmospheric and oceanic DA. These shocks (also evident for atmospheric–land DA) from the independent updating using disjoint information from these different components of the Earth system are a main disadvantage of the WCDA LDAS schemes (Penny et al. 2017).

A strongly coupled land–atmospheric data assimilation (SCDA) technique is possible, as demonstrated by Lin and Pu (2020), who used a full ensemble data assimilation method to update at least soil moisture (not temperature) as a control variable (also in Table 1). Despite representativeness limitations for in situ soil observations mentioned earlier, their study produced successful results and even used a convection-allowing (4-km grid spacing) model configuration. However, this SCDA method has not been implemented yet in the operational NWP models. Moreover, further evaluation of SCDA is needed, including assessment on if land–atmosphere SCDA might overly fit atmospheric observations at expense of soil measurements and not produce optimal results for nonatmospheric applications such as agriculture or hydrology.

A method presented in this study is a first step toward implementing a SCDA technique in the NOAA NWP regional models. It was developed out of a preexisting full 3D atmospheric analysis (including 2-m temperature and moisture observations), using its increment to infer an analysis increment for soil conditions (and for snow, where appropriate) rather than use a separate LDAS. It does not include assimilation of microwave (MW) satellite-sensed soil retrievals (e.g., SMOS, ASCAT, SMAP) and bypasses

TABLE 2. Earth system coupling introduced to NOAA hourly-updated regional models (HRRR, RAP, RUC). More information in section 3.

Component	Coupling via	Variables	Layers	Year		DA	Other
				introduced—expt	introduced—NCEP		
Soil	LSM	Temp, moisture	9 starting before 2012, 6 before	1996	1998	Cycling, atmos-to-soil DA	Moderately coupled land DA
Snow (on both soil and sea ice)	LSM	Water equivalent, temp, density	Up to 2	1997	1998	Cycling, atmos-to-soil DA, trim/build from satellite	Moderately coupled land DA Snow-free and snow-covered.
Sea ice	LSM	Temp	9	2010	2012	Specified from satellite	Subgrid fraction for sea ice from GFS, introduced 2018
Smoke	Atmos model	Smoke mixing ratio	50 (all) atmospheric layers	2017	2020	Cycling, fire radiative power from satellite	No direct DA, only cycling
Small lakes	Coupled lake model	Temp, ice, mixing	10 lake layers, 10 soil layers under the lake, up to 5 layers in snow	2018	2020	Cycling	No direct DA, only cycling
Large lakes (Great Lakes)	Separate lake model	Temp, mixing	FVCOM levels	2018	2020	Independent	FVCOM driven by HRRR wind, radar, temp, 6-h lag

difficulties with estimating surface emissivity at MW frequencies for a variety of land surfaces (Aires et al. 2011; Hirahara et al. 2020). Therefore, it is an interim solution but provides a benchmark for land DA techniques including MW data. For reasons to be explained below, we consider this a *moderately* coupled land DA (MCLDA) method, using a level of DA coupling between weakly and strongly coupled DA methods described by Penny et al. (2017). In weakly coupled DA methods, only 2-m observations are assimilated from the atmosphere in the LDAS. However, a previous observation impact study with the RAP model including MCLDA, James and Benjamin (2017, their Fig. 20), showed often equal impact and sometimes even larger impact (in summer daytime) on surface (2-m temperature and dewpoint) forecasts from upper-level observations (especially aircraft) than from DA of 2-m temperature/moisture observations themselves. This means that these upper-level observations are important contributors for land surface analyses.

3. Description of model framework (RAP and HRRR) for experiments

The hourly updated NOAA 13-km RAP and 3-km HRRR model–assimilation NWP systems provide a mesoscale environment to apply and test a high-frequency coupled data assimilation component. The short-range predictions from the HRRR (covering the lower 48 contiguous United States and Alaska at 3-km resolution) and from the RAP (covering North America and parts of Europe and Asia at 13-km resolution) are central for the NOAA NWP guidance out to 48 h for many applications including severe weather, transportation, energy, and hydrology (D22; J22; B16). For these applications, accurately predicted evolution of the boundary layer is essential; so much attention has been given also to accurate prediction of land surface conditions, which is necessary, in turn, for heat, moisture, and momentum fluxes.

a. Model

A cohesive set of subgrid-scale parameterizations (Table 3) has been developed and evolved for HRRR and RAP, including use of MYNN (Mellor–Yamada–Nakanishi–Niino) scheme for its boundary and surface layers (Olson et al. 2019a,b) including subgrid-scale cloud representation and a multispecies bulk cloud-microphysics representation (Thompson and Eidhammer 2014). The lowest computational level in HRRR/RAP is ~8 m above ground level (computational level at $\sigma = 0.999$, see Table 7 in B16). The configuration of parameterization suite is described in more detail by D22 and B16.

A component of the RAP/HRRR model is the RUC land surface model, a 9-layer soil–vegetation–snow model treating heat and moisture transfer including frozen soil conditions (Smirnova et al. 2000, 2016). The RUC LSM implements an implicit solution of heat and moisture budgets for a thin layer spanning the ground surface across a thin top layer in soil or snow and the lowest layer in the atmosphere (Smirnova et al. 1997). The RUC LSM is an LSM option for the WRF (Weather Research and Forecasting) community model (Skamarock et al. 2019) through which it has been widely

used in many WRF applications other than the NOAA HRRR/RAP models. RUC LSM has been evaluated in many soil- and snow-model intercomparisons, including ESM-SnowMIP (Krinner et al. 2018), and found to be an effective snow model compared to other international snow models (Menard et al. 2021) despite its intentional design choosing simplicity where possible. Fixed and surface fields (e.g., land use and albedo) are prescribed largely through MODIS datasets (Smirnova et al. 2016), with real-time-varying VIIRS-based greenness vegetation fraction, and use of the Beijing Normal University (BNU) soil dataset (Dy and Fung 2016). More details on the RUC LSM and its land-use fields are provided in He et al. (2021), especially in their Table A1.

b. Data assimilation

As short-range forecast models, the HRRR and RAP are especially dependent on effective data assimilation and both rely on a 1-h update frequency. The HRRR/RAP data assimilation (DA) uses a configuration of the NOAA community Gridpoint Statistical Interpolation (GSI; Kleist et al. 2009). The HRRR/RAP DA design includes a hybrid ensemble/variational assimilation (Hu et al. 2017) of in situ observations from rawinsonde and aircraft as well as satellite radiances (Table 4). It also includes unique components for 3D assimilation including 2-/10-m surface observations (B16), radar reflectivity and lightning stroke density observations (Weygandt et al. 2022; D22), and cloud/clear observations from satellites and surface-based ceilometers (Benjamin et al. 2021).

For the 3-km HRRR model, the same forward atmospheric DA is introduced from the 13-km RAP with a 1-h spinup cycle at 3 km (see D22). For both RAP and HRRR models, soil/snow conditions have been cycled over a multiyear period from early 1997 (Berbery et al. 1999), improved by the MCLDA soil/snow DA method described in this paper starting in 2004. Long-cycled soil temperature/moisture fields have been interpolated intermittently to new grids with next generations of NOAA hourly updated models to minimize LSM spinup. Thus, the soil state in 1997 from the Rapid Update Cycle (Berbery et al. 1999; Benjamin et al. 2004) has been continuously evolving into the 2021 RAP and HRRR land surface fields over the lower 48 contiguous United States using nearest-neighbor interpolation as needed when transferring to new model grids. Cycling of different Earth system components for RAP/HRRR models is described through Table 2.

Surface observations (2-m temperature, dewpoint) are incorporated directly within the full atmospheric DA for HRRR/RAP, different from the separate LDAS design used by other NWP models as shown in Table 1. This design for HRRR/RAP includes a forward model for surface observations with a correction to 2-m temperatures to account for the elevation difference between observation and model using local prognostic lapse rates (Benjamin et al. 2004). Furthermore, observation-minus-background innovations (Benjamin et al. 2010; James and Benjamin 2017) for temperature and moisture from surface

TABLE 3. Model physics and data assimilation configurations for the NOAA hourly-updated HRRR (3 km) and RAP (13 km) regional models. HRRR domains are the contiguous United States (CONUS) and Alaska (AK) domains (more detail in [section 3](#) and in [D22](#)).

System	HRRRv1/RAPv2	HRRRv2/RAPv3	HRRRv3/RAPv4	HRRRv4/RAPv5
Model	WRF-ARWv3.4.1+	WRF-ARWv3.6+	WRF-ARWv3.8.1+	WRF-ARWv3.9.1+
Domain	CONUS, North America	CONUS, North America	CONUS, North America, Alaska	CONUS, North America, Alaska
Initialization frequency	1 h	1 h	1 h, 3 h	1 h, 3 h
Map projection	Lambert conformal (CONUS), rotated lat/lon (North America)	Lambert conformal (CONUS), rotated lat/lon (North America)	Lambert conformal (CONUS), rotated lat/lon (North America), polar stereographic (AK)	Lambert conformal (CONUS), rotated lat/lon (North America), polar stereographic (AK)
Atmospheric vertical layers	51	51	51	51
Vertical coordinate	Sigma, lowest midlevel = 0.999	Sigma, lowest midlevel = 0.999	Hybrid sigma–terrain-following, lowest midlevel = 0.999	Hybrid sigma–terrain-following, lowest midlevel = 0.999
Soil levels	9	9	9	9
Horizontal/vertical advection	Fifth-order upwind	Fifth-order upwind	Fifth-order upwind	Fifth-order upwind + IEVA (see D22)
Computational horizontal diffusion	None	Sixth order (0.25)	Sixth order (0.25), horizontal only (not on slopes), applied to all variables	Sixth order reduced to 0.04 for tracers, including water vapor and hydrometeors, and to 0.12 for other model variables
Run frequency	Hourly	Hourly	Hourly, 3 h	Hourly, 3 h
Forecast duration	15 h	18 h	36 h every 6 h, otherwise 18 h	48 h every 6 h, otherwise 18 h
Land surface, including number of layers	RUC LSM, 9 soil levels, 2-layer snow (v3.5+)	RUC LSM, 9 soil levels, 2-layer snow, reduced wilting point (v3.6+)	RUC LSM, 9 soil levels, 2-layer snow (v3.8+)	RUC LSM, 9 soil levels, 2-layer snow (v3.9+)
Land parameters	30" MODIS land use, 30" STATSGO soil types, climatology for albedo, greenness, leaf area index (LAI)	Same as HRRRv1	Same as HRRRv2 but added real-time greenness vegetation fraction	Changed to 15" MODIS land use, BNU soil type (via WRF), MODIS albedo
Planetary boundary and surface layer	Mellor–Yamada–Nakanishi–Niino (v3.5+)	Mellor–Yamada–Nakanishi–Niino (v3.6+)	Mellor–Yamada–Nakanishi–Niino (v3.8+)	Mellor–Yamada–Nakanishi–Niino (v3.9+)
Subgrid-scale (SGS) clouds for radiation	None	MYNN RH-based (Benjamin et al. 2016, appendix B)	MYNN prognostic SGS cloud fraction, cloud water	MYNN removed limit to SGS cloud water, reduced radii
Radiation	RRTMG	RRTMG	RRTMG	RRTMG
Orographic drag	None	None	Small-scale orographic drag	Turbulent drag from subgrid orography (CONUS only)
Cloud microphysics	Thompson (v3.4.1)	Thompson–Eidhammer “aerosol-aware” (v3.6.1)	Thompson–Eidhammer “aerosol-aware” (v3.8)	Thompson–Eidhammer “aerosol-aware” (v3.8)

observations are used as additional observations via upward replication in the local boundary layer.

This overall hourly DA design in HRRR/RAP with components assimilating clouds, precipitation, and surface observations uniquely constrains the short-range prediction that drives the 0–1-h forcing for the land surface fields in HRRR/RAP, as

demonstrated by [J22](#). The DA here includes a snow-cover update component found to be effective and more effective for the RAP assimilation/model than those for other NCEP models ([Dawson et al. 2016](#)). Accurate fluxes are important even in the first model time step and certainly in the first prediction hour for the hourly updated HRRR/RAP models; more error is

TABLE 4. Observational data used in the RAPv5 and HRRRv4 3-d data assimilation (updated from Table 4 in B16). RH is relative humidity with respect to water, V refers to horizontal wind components, T is temperature, T_v is virtual temperature, p_s is surface pressure, T_d is dewpoint, q_v is water vapor mixing ratio, and p is pressure.

Data type	Variables	Frequency
Rawinsonde (including special obs)	T, RH, V, z	12 h
Boundary layer (915 MHz) profiler wind	V, T_v	1 h
Radar -VAD winds (WSR-88D radars)	V	1 h
Radar	Reflectivity, radial wind	1 h (or higher)
Lightning	Stroke density rate converted to reflectivity	1 h
Aircraft	V, T, q_v	1 h
Surface/METAR–land	V, p_s, T, T_d	1 h
Surface/METAR–land	Ceiling/visibility	1 h
Surface/mesonet–land	V, p_s, T, T_d	1 h
Buoy/ship	V, p_s	1 h
GOES atmospheric motion vectors	V, p	1 h
GOES cloud-top	p, T	1 h
AMSU-A/HIRS-4/MHS/GOES /IASI/ATMS/CrIS/SEVIRI	Radiances	1 h (or higher)
MODIS/VIIRS fire radiative power	Fire radiative power	1 h
GPS precipitable water	PW	1 h
Tropical cyclone vitals (TCVitals)	p_s	6 h
National Ice Center snow cover	Snow cover	24 h
National Ice Center ice cover	Ice cover	24 h

introduced by requiring the model to readjust by itself. Using an appropriate coupling of the data assimilation between land surface and atmosphere reduces initialization shock with both atmosphere and land–snow surface updated simultaneously. The evolution of the HRRR/RAP models since 2014 is provided in Table 3 here for users of HRRR/RAP data including land surface fields (see data availability statement). More details on the evolution of HRRR/RAP model and data assimilation are available in D22.

4. Design for moderately coupled DA for soil and snow variables

Land surface fields of temperature (for soil and snow) and volumetric moisture content (for soil only) are modified *vertically* in each column based on the full 3D atmospheric analysis increment extracted for the lowest model level. The evolution of data assimilation for the hourly updated NOAA models (RUC, RAP, HRRR) was to first develop a full 3D atmospheric assimilation including (e.g., B16) and then add a component to infer a soil increment (moisture and temperature). This is different from ECMWF and UKMO, who developed near-surface and soil LDAS capabilities separate from their atmospheric DA. In other words, the land surface analyses of this study as used in the NOAA HRRR and RAP models are affected by all available atmospheric measurements (e.g., soundings, aircraft, satellites, and 2-m screen-level data), while the land surface analyses in ECMWF and UKMO (and also from Météo-France and ECCO) assimilate only 2-m screen-level measurements and other soil-related satellite data. (We note that these LDAS analyses from these centers do use short-range forecasts that were previously affected by all observations.) Snow cover and ice cover are also modified *horizontally* based on satellite-based observations (entries in

Table 4). These two components comprise the land–snow data assimilation described in this paper.

We first describe the vertical component of the moderately coupled data assimilation technique presented in this paper. Only in this vertical component is the atmospheric data assimilation directly applied to the land/snow fields. The RAP and HRRR use the GSI data assimilation system (Kleist et al. 2009, B16). An extension of the GSI was developed to link the full soil/snow prognostic fields with the atmospheric prognostic fields during the data assimilation procedure (appendix A in B16).

After the atmospheric increment is calculated (hybrid variational–ensemble; Hu et al. 2017), increments for temperature fields in the multilevel [$T_s(k)$] soil are then calculated using

$$\Delta T_s(k) = \alpha_T(k)\Delta T_a, \tag{1}$$

where ΔT_a is the atmosphere temperature analysis increment at the model level closest to the surface and $\alpha_T(k)$ is the assumed correlation ratio for temperature for the k th soil or sea ice level, ranging from 0.6 at the top level down to 0.2 at the fifth level at 30-cm depth (see Table 5). A value of $\alpha_T(k = 1)$ of 0.6 reduces the postanalysis soil–atmospheric temperature contrast by 60%, reducing initial flux shock (more in section 6). The term $\Delta T_s(k)$ is the soil temperature increment (K) at the k th soil or sea ice level. The soil or sea ice temperature analysis increment applied in each analysis is limited to maximum value of 1.0 K and to a minimum value using

$$\min\Delta T_s(k) = -2.0 \times f \times 0.6, \tag{2}$$

where $f = 1 + \min\{1.5, \max[0, (T - 283.0)/15.0]\}$ and where T is the first model level air temperature. Values of T used in f are bounded to 283–305 K. Below 283 K, f is set = 1.0 and $\min\Delta T_s(k) = -1.2$ K, and above 305 K, f is allowed to be larger and set as 2.5, and $\min \Delta T_s(k) = -3$ K. The larger

TABLE 5. Estimated correlations [$\alpha_T(k)$] between forecast error for soil temperature and near-surface atmospheric temperature [Eq. (1)] as a function of the k level in the land surface model.

k	$\alpha_T(k)$ for 9-level soil configuration	Soil depth (cm) for 9-level configuration
1	0.60	0
2	0.55	1
3	0.40	4
4	0.30	10
5	0.20	30
6	0	60

negative increment threshold is appropriate for nighttime conditions especially in winter.

If snow cover is present in the background field and covers the grid cell at a given grid point partially, the skin temperature and snow temperature at the interface between the two layers in the RUC snow model (Smirnova et al. 2016) are also modified with the same relationship used in (1) and (2). The snow temperature cannot be increased over 273.15 K.

Next, an analysis increment for soil volumetric water content [$\Delta\eta_s(k)$] is calculated during daytime only also from the atmospheric analysis increment as

$$\Delta\eta_s(k) = \alpha_\eta(k)\Delta RH_a, \tag{3}$$

where ΔRH_a is the analysis increment of atmosphere relative humidity (calculated from temperature and water vapor mixing ratio background fields and newly analyzed fields) at the lowest model level, $\eta_s(k)$ is the soil volumetric water content limited by porosity for the given soil type (Smirnova et al. 1997, 2016) in dimensionless units ($m^3 m^{-3}$) and defined at each k th soil level, and $\alpha_\eta(k)$ is the assumed correlation ratio for moisture for the k th soil level. ΔRH_a is limited to range from -0.15 to 0.15 . Similar ensemble-based correlations were found by Mahfouf (1991) and Lin and Pu (2018) with a different coarser land surface models than used for HRRR and RAP (Table 6). Application to soil moisture using MCLDA only in daytime (since correlation expected only during an active boundary layer) is consistent with coefficients found by Lin and Pu (2018) for daytime versus nighttime (larger in daytime, near zero at night, Table 6 here).

For a 9-level soil model configuration, a correlation between the atmospheric moisture increments and the soil moisture increments is assumed down to the top four levels (down to 10 cm) with parameters shown in Table 6. The correlation factors $\alpha_\eta(k)$ have nonzero values only during daytime [$\cos(\text{solar zenith angle}) > 0.3$] and when there is no snow cover. A soil moisture increment is applied only when atmospheric temperature and RH increments are of opposite sign and when the atmospheric temperature analysis increment at a given grid point at the lowest atmospheric level $|\Delta T_a| > 0.15$ K. This treatment is consistent with the negative correlation between soil moisture and near-surface temperature forecast error found by Mahfouf (1991) and mainly in daytime by Lin and Pu (2018, their Fig. 6) but a stricter condition (requiring opposite-sign

TABLE 6. Estimated correlations [$\alpha_\eta(k)$] between forecast errors of near-surface humidity and soil moisture [Eq. (3)]. Values shown for daytime and nighttime. Also, in the three rightmost columns: correlation factors for analysis increments between atmosphere and soil moisture at 4 layers (k) from Lin and Pu (2018, Fig. 6), also varying for day vs night, and from Mahfouf (1991, Table 2) for a single layer for different local times (LT).

k	$\alpha_\eta(k)$ for 9-level configuration		$k/\text{depth of soil layers (cm)}$: Lin and Pu (2018), Noah LSM 4-layer config	Lin and Pu (2018, Fig. 6f): $Q-Sm$ correlation—nighttime	Lin and Pu (2018, Fig. 6e): $Q-SM$ correlation—daytime	Mahfouf (1991, Table 2): RH- w_p
	Daytime	Nighttime				
1	0.2	0	1/10	0.07	0.23	0.54 (0600 LT) -0.87 (1800 LT)
2	0.2	0	1			
3	0.2	0	4			
4	0.1	0	10			
5	0	0	30		—	N/A
6	0	0	60		—	N/A

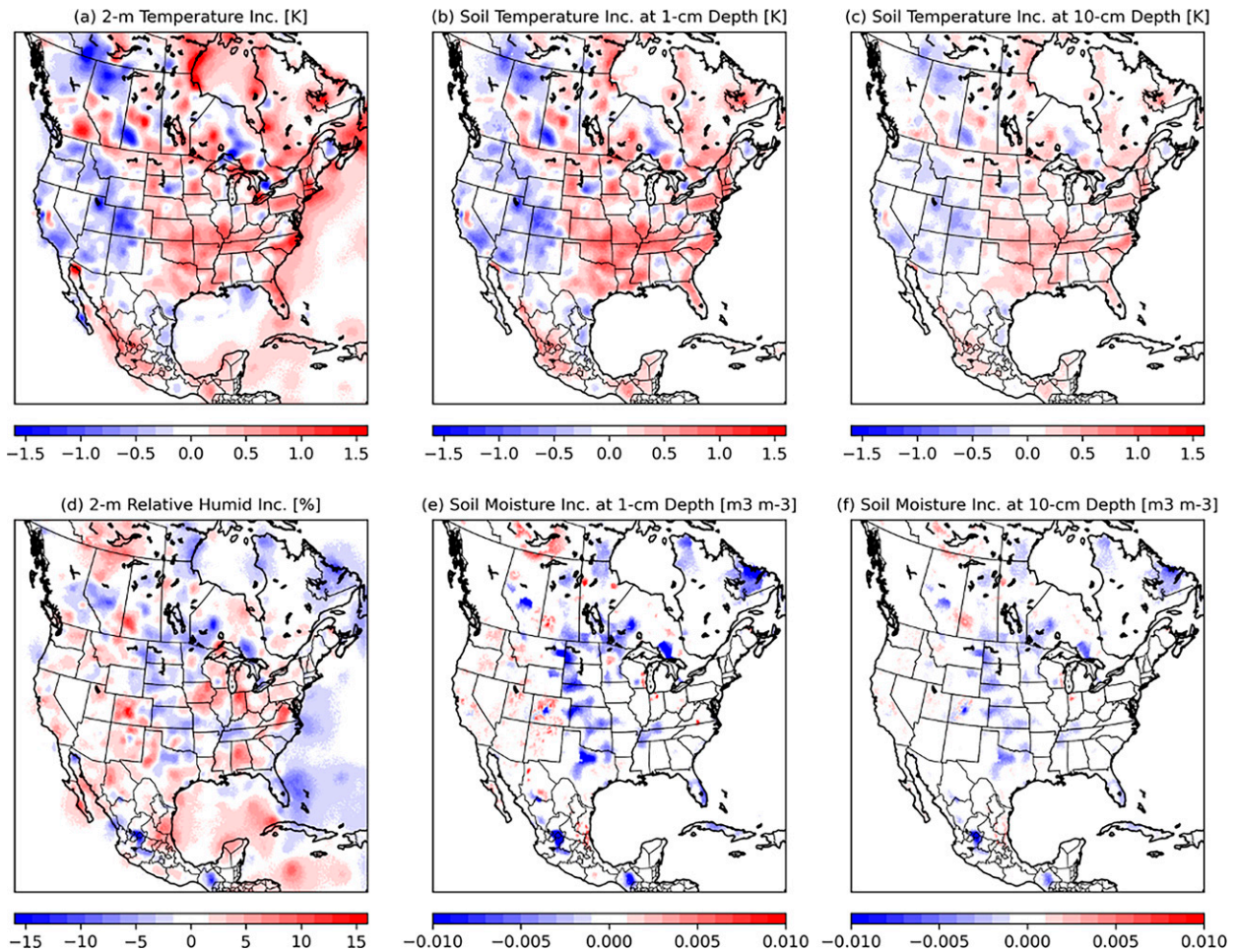


FIG. 1. Example of temperature and moisture analysis increments using MCLDA for both atmosphere and soil for the same time in hourly 13-km RAP/GSI assimilation cycle at 1500 UTC 12 Jul 2019.

atmospheric temperature/RH increments) in the technique shown in this paper. The soil moisture analysis increment applied in each analysis is limited to maximum value of 0.03 and to a minimum value of $-0.03 \text{ m}^3 \text{ m}^{-3}$.

The soil moisture increment design in MCLDA is based on the assumption that Bowen ratio (between sensible and latent heat fluxes, e.g., Monteith 1973) errors related to soil moisture errors produce opposite atmospheric errors of near-surface temperature and moisture. A warm/dry bias in the atmospheric near-surface forecast is often caused by or at least associated with too-low soil moisture, and a cold/moist near-surface atmospheric bias is often associated with too-high soil moisture. This overall cross-variable daytime-only dependency used in our method is very consistent with the cross-variable correlations for forecast errors for 2-m temperature and 2-m humidity in daytime. Similarly with the ensemble-based forecast error covariances found by Lin and Pu (2020), their Fig. 6a) and Lin and Pu (2018, their Figs. 6e,f), a soil moisture error was found to be inversely correlated with near-surface atmospheric temperature errors. A similar opposite relationship in 2-m temperature and 2-m moisture errors related to soil moisture errors was found

by Mahfouf (1991). In his Table 2, similar correlations between soil moisture and near-surface temperature ($\rho_{ws,T}$) were found to range from about -0.5 to -0.9 . Mahfouf (1991) also found that the atmosphere is not informative during cloudy or precipitating periods when downward solar radiation is small and coupling with the underlying surface is weak. This condition is roughly similar to the requirement for opposite signs of increments for near-surface temperature and near-surface RH in our method.

We consider the described technique as a moderately coupled land data assimilation (MCLDA), a step forward from a WCDA technique toward SCDA. The atmosphere and land or snow variables are both updated within the same DA using the same full set of atmospheric observations (Table 4). Hourly assimilation of 2-m temperature and dewpoint observations within the atmospheric DA are a critical enabler for MCLDA, but this has been routine for the GSI-based DA for RAP and HRRR (B16, James and Benjamin 2017).

An example of soil temperature and moisture analysis increments for daytime (1500 UTC) during 12 July 2019 using the described MCLDA technique is shown in Fig. 1. Soil temperature increments are much more widespread than moisture

increments and are related directly to the 2-m temperature increment (diagnosed from lowest model level increment) shown on the left in this figure. Application of MCLDA for soil (or ice or snow) temperature increments has no dependency on time of day while for soil moisture MCLDA is not applied at night. The soil moisture increments shown in this example are related to the 2-m atmospheric RH increment (not exactly the lowest-level (8 m AGL) RH used in MCLDA but very close to it) but are constrained and are not applied without opposite signs of 2-m temperature and 2-m RH atmospheric increments. For example, the region along the Iowa–Illinois border has positive RH increments (Fig. 1d); however, due to MCLDA constraints, the soil moisture does not have any moistening in this region. For both soil temperature and soil moisture, the increment's magnitude decreases for deeper soil levels, consistent with the $\alpha_7(k)$ correlations for temperature shown in Table 5 and the $\alpha_7(k)$ correlations for moisture shown in Table 6.

5. Horizontal snow cover modification

The MCLDA is applied for snow-covered grid points in the land surface conditions and for temperature only. As part of the overall land surface updating process (assimilation in a broad sense), changes in *horizontal* snow cover are also applied once per day at 0000 UTC using daily products (valid ~2300 UTC) of Northern Hemispheric snow and ice cover (Table 4) provided by NOAA (U.S. National Ice Center 2008; Helfrich et al. 2007). The Interactive Multisensor Snow and Ice Mapping System (IMS¹) data are used as part of this overall land–snow assimilation. The IMS-Snow data are available at 4-km resolution over the entire Northern Hemisphere and based on data from polar-orbiting and geostationary satellites.

The IMS-Snow data are interpolated to the 13-km RAP grid or the 3-km HRRR grid, both of which have prior information on snow cover, snow temperature, and snow water equivalent (SWE) from the 1-h cycling of those models including assimilation of radar and satellite-cloud data (see section 3b). Snow building is applied at grid points when IMS-Snow indicates snow cover present and the model background showed none, and also when the lowest-level atmospheric temperature is <278 K. In this case, the snow-building algorithm searches for nearby grid points (up to ± 2 points in each direction) with snow, determines the mean SWE for these nearby points, and adds this mean SWE to the grid point without prior snow. This procedure compensates for possible spin-up problems in the 1-h model snow precipitation or for misplaced snow precipitation. When there are no adjacent snow-covered points, a small amount of SWE (1 mm) is added to the grid points that should have snow cover, enough to survive daytime heating of a few hours. For points with added snow cover, skin temperature and soil temperature at the top three levels are reduced, if needed, so that these temperatures do not exceed 272 K. If the IMS-Snow data indicate that

model grid points should not have snow and requiring clearing, this is only performed under the condition that the model has shown no precipitation during the previous hour. (In this case, the IMS-Snow data indicating that clearing is needed may have become obsolete at that grid point over the last hour.) The trimmed snow is relocated to adjacent grid points with missed snow cover if they exist to preserve conservation of water.

IMS-Snow data are also applied similarly for clearing and building by other NWP centers (Table 2) including ECMWF (de Rosnay et al. 2014), UKMO (Pullen et al. 2011), and both Canadian and French NWP systems (Bélair and Boone 2020). These NWP centers use this dataset only for revising horizontal snow cover, part of a two-step procedure with a separate initialization for snow depth and SWE (e.g., de Rosnay et al. 2014).

A comparison of SWE fields is shown in Fig. 2 from two experiments using the NOAA RAPv5 model with (Fig. 2a) and without (Fig. 2b) application of the overall land–snow DA including MCLDA and use of the IMS-Snow snow-cover modification. There are small differences over areas of the western United States (e.g., Oregon and Nevada), with greater snow cover in the DA simulation over many areas. A comparison is also provided in Fig. 2c with the SWE from the NOAA National Snow Analysis (NSA; see National Operational Hydrologic Remote Sensing Center 2004), showing more agreement with the MCLDA/snow-update SWE field in these areas of small differences. The general accuracy of the snow cover and SWE fields even in the no-MCLDA experiment is attributable to the other data assimilation methods (clouds, radar, etc.) used in the RAP and HRRR hourly cycles as described in section 3b and the accuracy of physical parameterizations including the land surface and boundary layer schemes as described in section 3a.

6. Experiments to assess effect of MCLDA/snow modification

In this section, results from experiments with and without the land–snow assimilation during two seasons are presented.

A set of Rapid Refresh assimilation–forecast experiments in both summer and winter was conducted to test the effectiveness of the MCLDA/snow data assimilation. These experiments were conducted over 1-month periods for 18 July–16 August 2018 for the summer period and for 1 February–1 March 2019 for the winter period (Table 7). The 13-km RAPv5 (implemented at NOAA/NCEP in December 2020) was used for all of these experiments with all other data assimilation and modeling configurations the same (as described in section 3) for experiments with and without the MCLDA/snow DA. Initial conditions for these 1-month experiments used RAPv5 conditions including evolved land fields with MCLDA/snow DA.

These experiments were evaluated primarily with atmospheric observations of temperature and dewpoint at 2 m (“2mT” and “2mTd,” respectively) and rawinsondes. RMS errors were calculated for each pair of experiments (MCLDA and noMCLDA). The figures in this paper present *differences* in RMS errors

¹ <https://usicecenter.gov/Products/ImsInfo>.

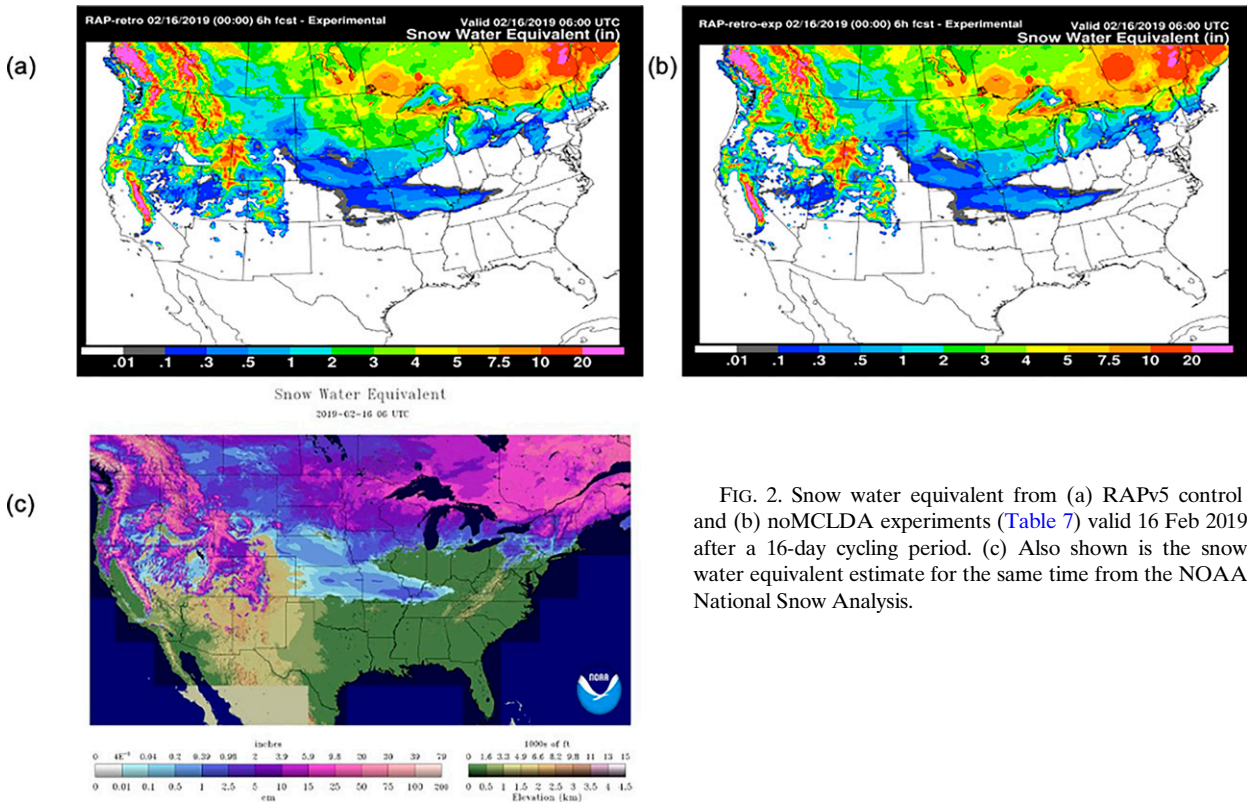


FIG. 2. Snow water equivalent from (a) RAPv5 control and (b) noMCLDA experiments (Table 7) valid 16 Feb 2019 after a 16-day cycling period. (c) Also shown is the snow water equivalent estimate for the same time from the NOAA National Snow Analysis.

between the pair of experiments and biases against these variables for both experiments. Figure 3 shows the difference in the RMSE relative to METAR observations as a function of both forecast length (1–24 h) and time-of-day (“valid time”), as well as the bias in 6-h forecast over valid time, results for the *summer-time* comparison. Because of the strong differences in terrain across the continental United States, the statistical results are separated into “eastern United States” (east of 105°W) and “western United States” areas. Figures 3a and 3b demonstrate that the forecasts that use MCLDA have smaller RMSE values than the forecasts where the surface properties were not updated via the MCLDA approach; samples that are statistically significant are indicated with black dots. The strongest impacts for reduced summer 2mT RMSE are at 0900, 1200, and 1500 UTC (late night to morning). This is true especially during the nighttime in the eastern United States (significant out to 6 h and even out to 15 h for forecasts valid at 1200 UTC) and especially in

morning hours in the western United States (significant out to 24 h). Furthermore, the bias in the summer 2mT (Figs. 3c,d) are also smaller when MCLDA is used. The warm bias for 2mT (at 6 h) is decreased at night and especially for the western United States (Figs. 3c,d). A daytime cold bias in the eastern United States is also decreased by MCLDA (Fig. 3c). During nighttime, the 2mT improvement from application of MCLDA is confined to the shallower boundary layer near the surface and with some residual into the mornings hours, especially in the western United States (Figs. 3b,d). These figures include the initial spindown period for the first few days as the noMCLDA cycle evolved from initial fields with MCLDA, so are slightly muted.

The effect of MCLDA on 2mTd RMSE in summer (Fig. 4) is positive (especially in the western United States, Fig. 4b) in the summer and only very slightly positive in the east (Fig. 4a). For the western United States, the 2mTd RMSE improvement

TABLE 7. RAPv5 cycled experiments for testing the moderately coupled land data assimilation (MCLDA) technique to modify soil/snow conditions. Hourly data assimilation was performed with forecast duration out to at least 3 h and up to 24 h every 6 h. These experiments were carried out for winter (February 2019) and summer (July–August 2018) periods as explained in text.

Expt No.	Expt name	Expt purpose	Application of MCLDA to soil and snow	Daily revision of snow cover with IMS Snow
1	MCLDA	Control, with MCLDA and land–snow DA	Yes	Yes
2	NoMCLDA	No MCLDA or land–snow DA	No	No

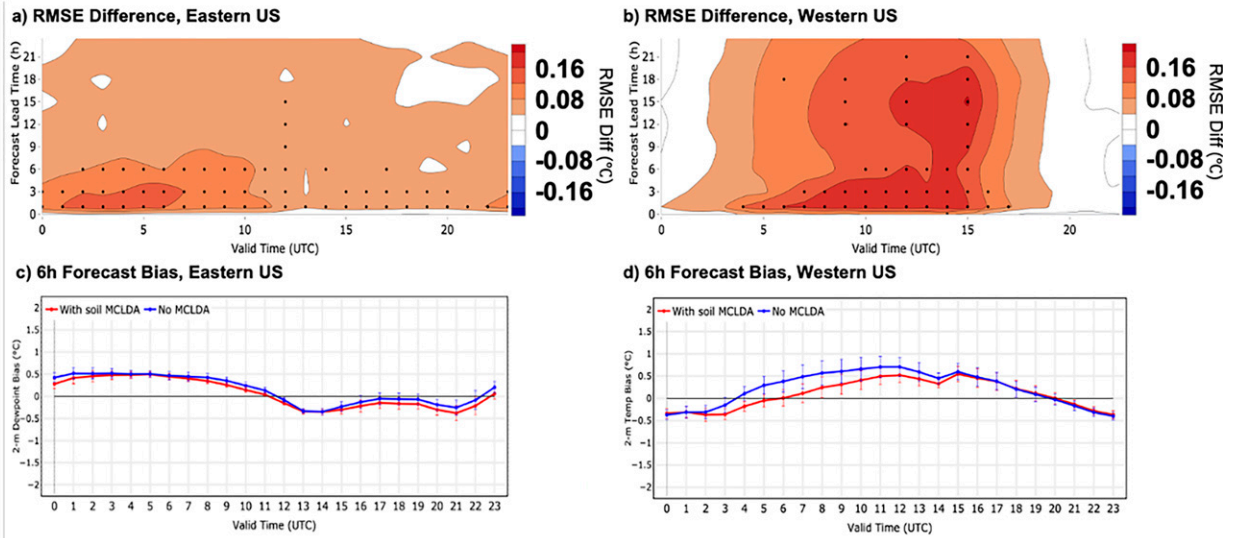


FIG. 3. RAP 6-h forecast skill for 2-m temperature in summer experiments with and without MCLDA (Table 7). (a),(b) RMS error differences for no-MCLDA minus MCLDA experiments. RMS errors vs METAR observations are calculated using the NOAA MATS (Turner et al. 2020). Differences in RMS error between noMCLDA and MCLDA experiments are plotted by valid time of day (horizontal axis) and forecast duration (vertical axis). Black dots are shown for 95% significant differences. (c),(d) Bias vs 2-m temperature observations is shown for both MCLDA and noMCLDA experiments for the same period. Panels (a) and (c) are for the eastern United States (east of 100°W) and (b) and (d) are for the western United States. Forecasts were run out to 6 h on an hourly basis and out to 24-h duration every third hour. For the study domain, the nighttime is approximately during 00000–1200 UTC while the daytime is during 1200–2400 UTC.

is during the daytime and into the early evening hours (Fig. 4b). An overall dry bias for 2mTd for 6-h RAP forecasts in the west was slightly decreased by application of MCLDA (Fig. 4d). Dewpoints (2mTd) are drier in the eastern United States with MCLDA applied (Fig. 4c), which is an improvement during

the overnight hours. There are two factors involved with the diurnal variation of the MCLDA impact—the diurnal variation of the boundary layer itself and the MCLDA design constraint to not allow soil moisture increments at night.

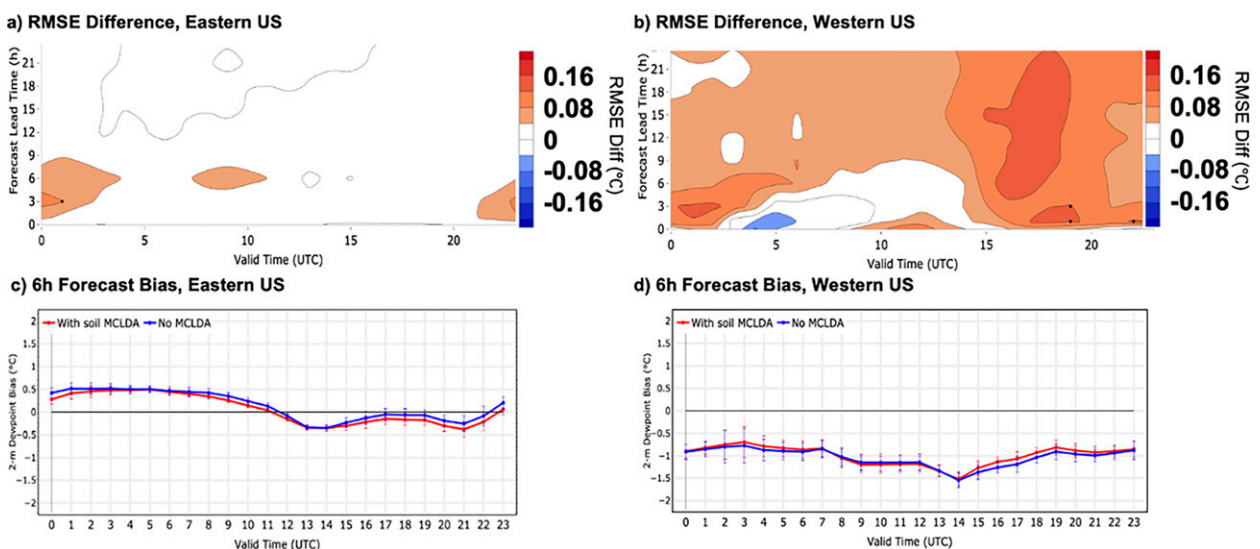


FIG. 4. As in Fig. 3, but now for 2-m dewpoint forecast skill, again for the summer experiment period and again for 6-h forecasts.

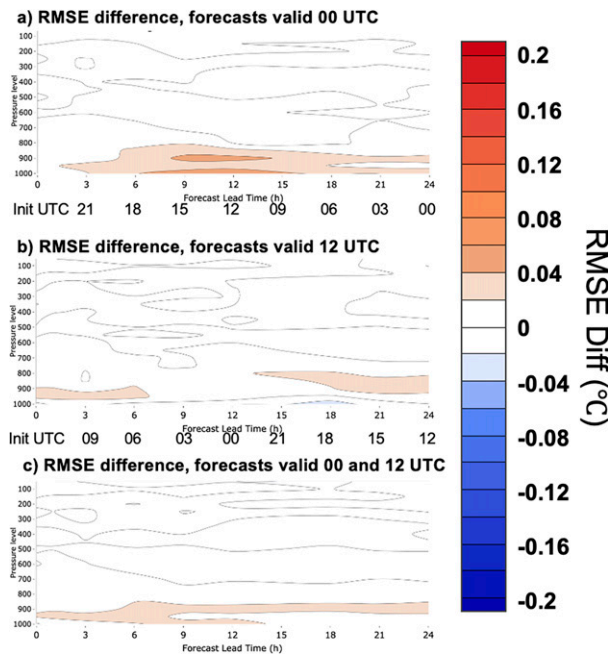


FIG. 5. Forecast skill difference for temperature vs rawinsondes between the same two experiments for the summer period as described in Fig. 3 and Table 7. The vertical axis shows the pressure level, and horizontal axis shows forecast duration or lead time. Initial time for 3-h, 6-h, etc. forecasts valid at (for example) 0000 UTC are also shown (2100 UTC, 1800 UTC, etc.). The valid time is fixed (0000, 1200 UTC) in each graphic. Graphics are shown for forecasts (a) valid at both 0000 and 1200 UTC, (b) valid at 0000 UTC only, and (c) valid at 1200 UTC only.

An evaluation of summer temperature forecasts, using RMSE differences between the two forecast configurations as a function of both height and lead time, was also made against rawinsonde data (Fig. 5) to inspect the depth of MCLDA

impact. Since rawinsonde data are available only twice daily, plots in Fig. 5 are shown with the *x* axis reflecting lead time (initial time also shown) for forecasts valid at 0000 UTC only (Fig. 5a), 1200 UTC only (Fig. 5b), and 0000 and 1200 UTC combined (Fig. 5c). A slight improvement is shown for approximately the 1000–800-hPa layer especially for forecasts valid at 0000 UTC (Fig. 8a, daytime) that are initialized at 0900–1800 UTC (i.e., those with a lead time of 6–15 h). This suggests that improvement in soil conditions in summer in the lower troposphere from MCLDA had the most important effect during the morning period with growth of the planetary boundary layer (PBL). This is consistent with the timing of maximum improvement of 2mT and 2mTd predictions in the western United States (Figs. 3b and 4b).

A similar analysis to evaluate the impact of the MCLDA and snow modifications (henceforth we will use “MCLDA” for both) was performed for the winter period (Fig. 6). For the winter experiment period for 2mT, the impact from MCLDA was also uniformly positive at all times of day and for 1–24 h, with the magnitudes of the reduction in RMSE even larger than for the summer period. In winter, improvement (reduction in RMS error versus METARs) from MCLDA for 2mT prediction (Fig. 6a) was as large as 0.12K (larger than in summer), significant at 1–3 h at all times of day, and significant out to 9–12 h at 1200–1500 UTC in the eastern United States (Fig. 6a) and out to 3–5 h in the western United States (Fig. 6b). The reduction in 2mT RMSE from MCLDA was matched by a notable decrease in 2mT bias from MCLDA at all times of day, especially in the eastern United States (Figs. 6a,c). The eastern United States reduced 2-m cold bias in winter from MCLDA is fairly strong (by 0.2°–0.4°C, Fig. 6c), significant or almost so at all times of day.

For 2mTd in winter (Fig. 7), 2mTd forecast improvement from MCLDA was very evident and focused sharply during afternoon-to-evening hours (1800–0000 UTC) for both east-

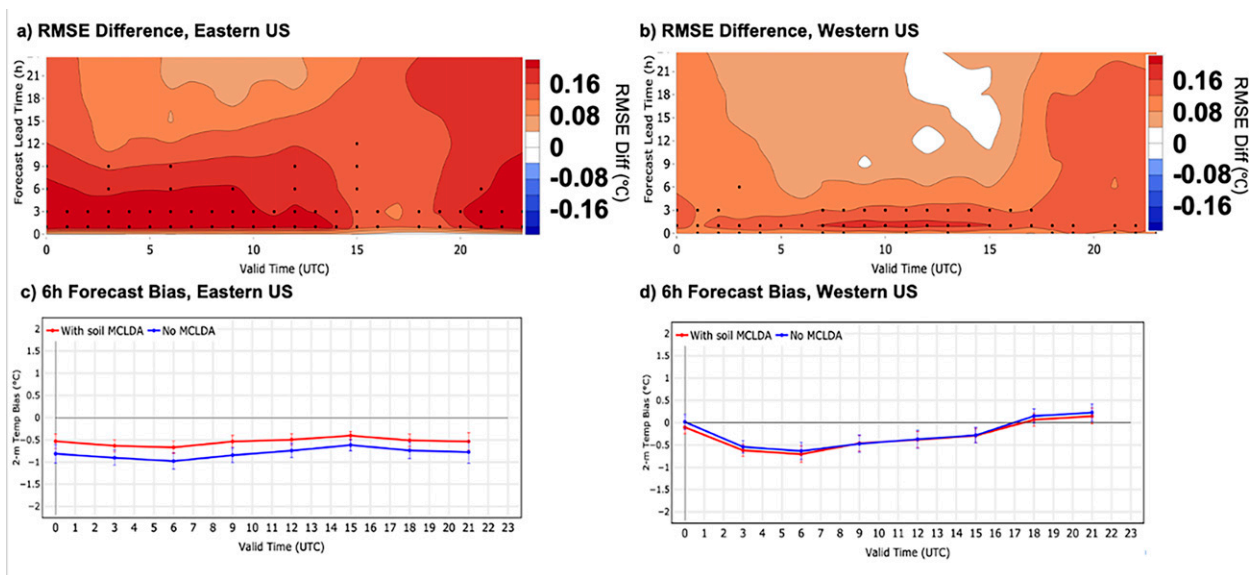


FIG. 6. As in Fig. 3, but for forecast skill against 2-m temperature but for 4-week winter experiments during February 2019, again with noMCLDA and MCLDA experiments.

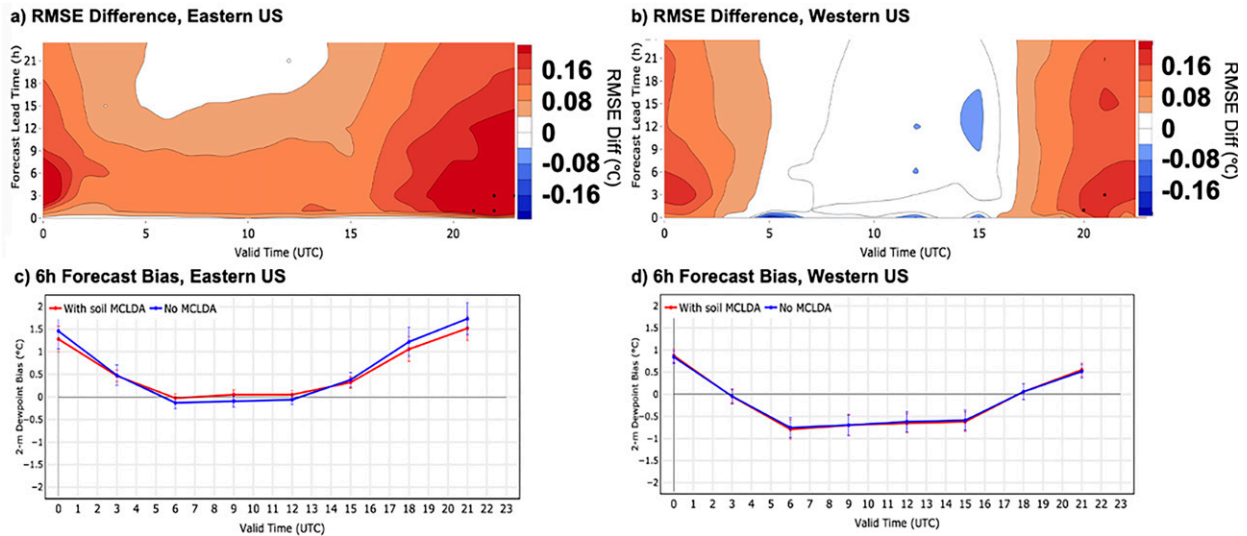


FIG. 7. As in Fig. 4, for 6-h forecast skill for 2-m dewpoint but for winter experiments.

ern (Fig. 7a) and western United States (Fig. 7b), significant out to 3-h forecasts for these times. This behavior, especially for winter, is considered to be related to the diurnal variation of the boundary layer depth. The moist bias in eastern United States was also improved by 0.2°–0.3°C in the daytime hours (Fig. 7c). Little change in winter in 2mTd bias (Figs. 7c,d) from MCLDA was evident.

A positive effect from MCLDA for temperature in the lower troposphere (1000–850 hPa) was stronger in winter (Fig. 8) than in summer (Fig. 5), similar to the larger effect

on 2mT in winter (Fig. 6) than summer (Fig. 4). Breaking out by valid time (0000 UTC, Fig. 8a; 12000 UTC, Fig. 8b) shows that the most pronounced positive effect from MCLDA is at 0000 UTC (Fig. 8a) from forecasts initialized 6–18 h prior (1800–0600 UTC). For 1200 UTC valid time, the impact from MCLDA is smaller and is mostly from forecasts with 1–6-h lead time (i.e., initialized overnight at 1100–0600 UTC).

Overall, a positive effect of the MCLDA soil/snow assimilation on temperature predictions was most evident, at least statistically, under more stable conditions, which are more common in winter, during the night, and in the early morning hours during summer. The effect of MCLDA is cumulative within the forward RAP data assimilation cycle, of course. The effect of presumably more accurate sensible flux from MCLDA is more focused in a shallower boundary layer at night and in winter but is apparently more diffused in the daytime deeper boundary layer, especially during afternoon in summer. For moisture, the largest impact is for forecasts valid during the afternoon hours with the strongest land–atmosphere coupling.

Figure 9 shows the hourly variation of 6-h forecast skill for 2mT and 2mTd with and without the land–snow DA for a 1-week period during the winter. Generally, 2mT RMS errors in eastern United States are reduced at all times of day by MCLDA (Fig. 9a, red), while improvements to 2mTd errors (also in Fig. 9a, blue) are most evident in daytime when the errors are the highest in their diurnal cycle. This pattern of 2mTd RMS errors justifies the design of MCLDA when soil moisture is adjusted only during the daytime hours when its impact on the surface layer moisture is the largest. For this winter period, the cold (2mT) and moist (2mTd) biases (both in Fig. 9b) are both reduced by the land–snow DA including MCLDA. The 2 m cold bias for 2mT was reduced by MCLDA over all times of day for this period.

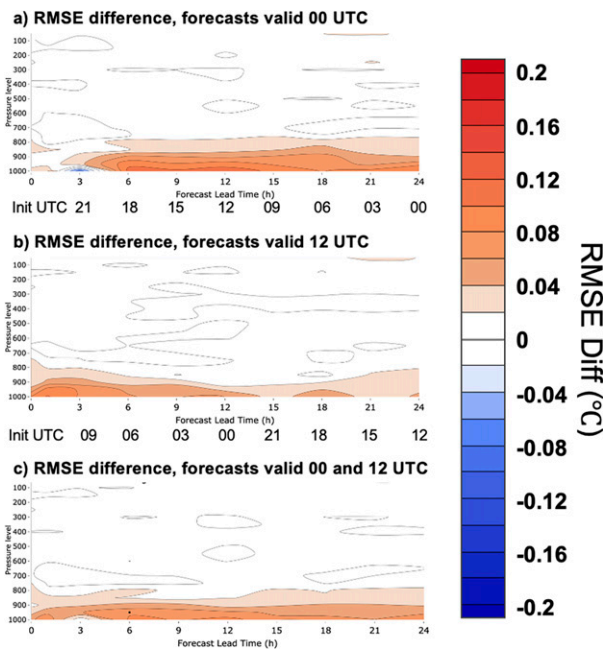


FIG. 8. As in Fig. 5, but for winter experiments.

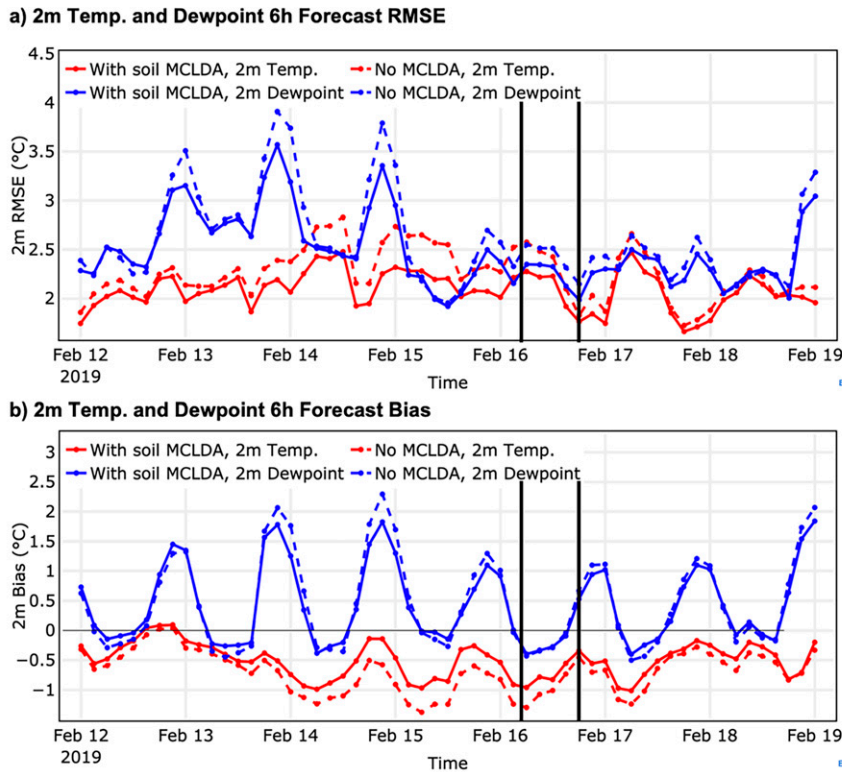


FIG. 9. Forecast error for 2-m temperature (red) and 2-m dewpoint (blue) over eastern United States for RAP model experiments with MCLDA (solid) and without MCLDA (dashed) for a week (12–18 Feb 2019) within the winter test period. (a) RMS errors, and (b) the bias errors. Vertical lines show the date of snapshots (16 Feb 2019) shown in Fig. 2 (0600 UTC) and Figs. 10 and 11 (1800 UTC).

The vertical lines in Fig. 9 correspond to the same date for a specific analysis increment comparison shown in Fig. 10 and for the snow-cover state in Fig. 2. For this time, the improvement from MCLDA in both RMS error and bias in 2mT in Fig. 9 are quite substantial while neutral for 2mTd. Although the snow cover patterns are very similar in eastern United States for this day (Fig. 2), the soil moisture and temperature at 1-cm depth (Figs. 10c,d) show large differences over eastern United States after two weeks of cycling with and without MCLDA starting with the same initial conditions. There are many regions where the soil temperature is markedly (2–4 K) colder when MCLDA is not used (e.g., Florida, Missouri, West Virginia, and Michigan), and in these areas the soil is also 0.10–0.12 m³ m⁻³ moister without MCLDA; this is consistent with 2mT and 2mTd RMS errors and biases shown in Fig. 9. A comparison of analysis increments for 2mT for the same time is shown in Fig. 11, with MCLDA (Fig. 11a) and without MCLDA (Fig. 11b). Both analysis increments are positive over the eastern United States as the assimilation warms up the too-cold 1-h forecast, but the analysis increment is larger without MCLDA (Fig. 11b).

We also made careful comparisons of latent and sensible heat fluxes for a midday time (1800 UTC) for MCLDA and noMCLDA experiments from 15 August 2018 during the

summer test period. Our goal was to investigate for any “shocks” in fluxes from imbalance in initial soil and atmospheric temperature and moisture without MCLDA, similar to the ocean-atmosphere initialization shock studied by Mulholland et al. (2015). The latent and sensible heat fluxes (LHF, SHF) for 1801 UTC (after a single 1-min time step) are presented in Fig. 12, with larger latent heat fluxes in both experiments over the eastern United States where soil moisture is generally higher, and larger sensible heat fluxes generally over the western United States. Both flux estimates were affected by recent precipitation over western Mexico and Arizona (southwest monsoon) and the U.S. East Coast resulting in increased LHF and decreased SHF. Differences (MCLDA minus noMCLDA) are shown for LHF in Fig. 13a and for SHF in Fig. 13b. In many of the LHF maximum areas (>400 W m⁻²) with apparent recent precipitation (e.g., OK, FL, east coast), application of MCLDA increases LHF. For one of these points in central PA, a time series of LHF for the first 20 time steps of this model run (Fig. 13c) shows a sudden drop (shock) for the noMCLDA experiment with an LHF decrease of ~100 W m⁻² in the first time step. By contrast, with a more balanced initial state in the MCLDA run, the first time step only shows a decrease of ~10 W m⁻², a much reduced shock. During the forecast the two runs slowly grow closer at this point, reducing

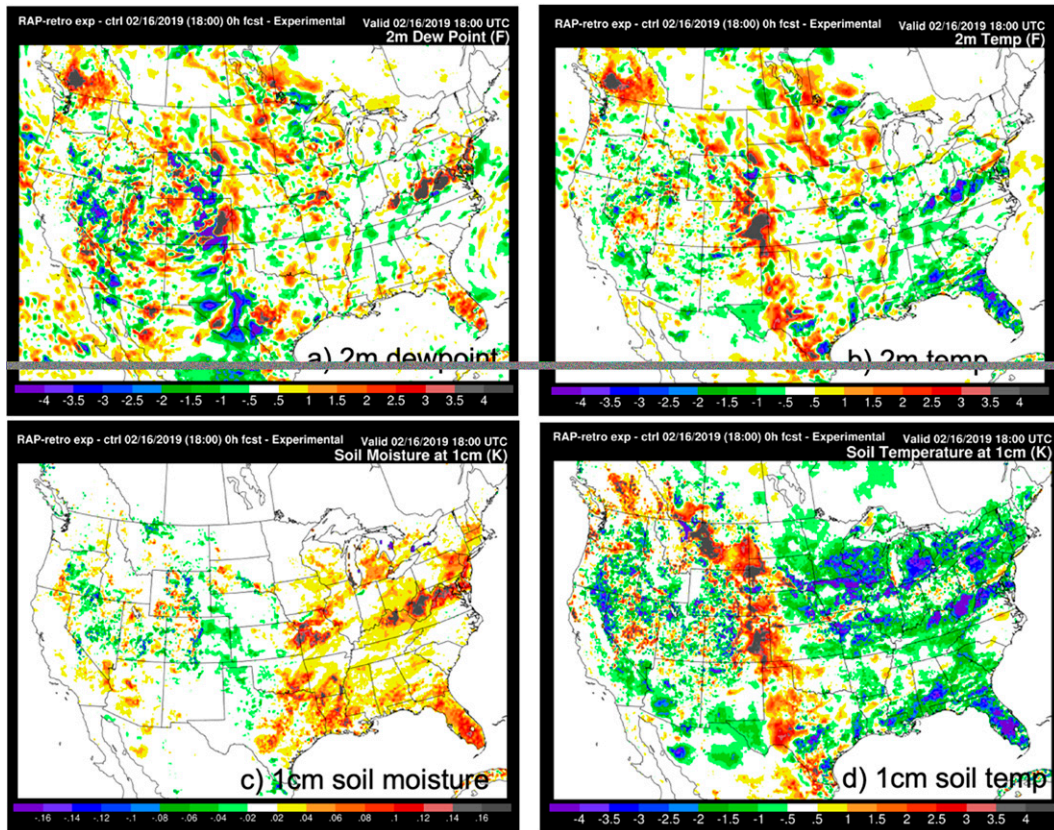


FIG. 10. Difference fields for MCLDA experiments (noMCLDA minus control with MCLDA) at 16 Feb 2019 1800 UTC. Differences are shown for (a) atmospheric 2-m dewpoint, (b) 2-m temperature, (c) soil volumetric moisture content ($\text{m}^3 \text{m}^{-3}$) at first level below surface (1-cm depth), and (d) soil temperature (also at 1 cm).

the difference in LHF from $\sim 100 \text{ W m}^{-2}$ at time step 2 to $\sim 50 \text{ W m}^{-2}$ after 20 min of integration, but still the noMCLDA experiment remains drier.

Sensible heat flux over this summer midday case after one time step was generally lower with MCLDA (Fig. 12b vs Fig. 12d, Fig. 13b), with somewhat less area with MCLDA showing at least 300 W m^{-2} in the western United States.

A point over northern California was selected for a time series comparison (Fig. 13d), showing a very large SHF shock of 400 W m^{-2} at the first time step for the experiment without MCLDA, but little perturbation with MCLDA. Without MCLDA, a strong negative atmospheric temperature increment but without any change to the soil temperature had resulted in the spike in SHF. Overall, the primary

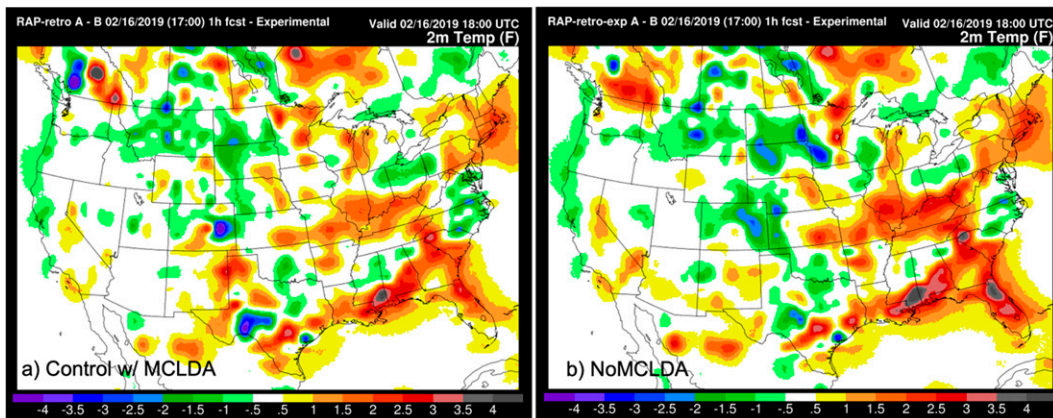


FIG. 11. The 2-m temperature analysis increments from (a) control with MCLDA and (b) noMCLDA experiments for 1800 UTC 16 Feb 2019.

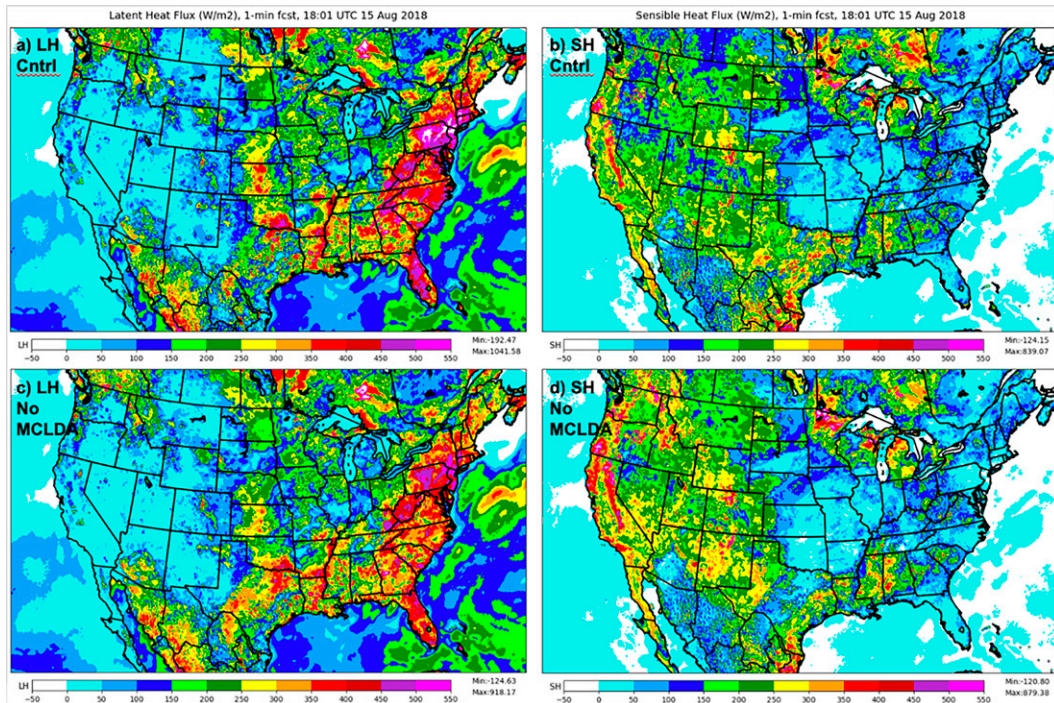


FIG. 12. Latent and sensible heat fluxes valid at first time step (1 min) from RAP experiments with and without MCLDA (only CONUS area shown). Valid at 1801 UTC 15 Aug 2019. (a),(c) Latent and (b),(d) sensible heat flux for control with MCLDA and noMCLDA experiments, respectively.

shocks without MCLDA shown in Figs. 13c and 13d last only a single time step, far less than the 12-h initialization shock for ocean shown by Mulholland et al. (2015). However, some difference in LHF and SHF at these grid points continued through the first 20 time steps (and beyond). The ongoing hourly assimilation in RAP, with cumulative minimizing of these hourly shocks via application of MCLDA, results in the improvements in 2mT and 2mTd and lower-troposphere temperature evident in Figs. 3–9.

7. Conclusions

Accurate land surface evolution is critical for determining land–atmosphere fluxes of heat, moisture, and momentum, which are in turn important for weather prediction on short-, medium-, and longer-range time scales. Initialization of land surface fields (soil and snow temperature, volumetric soil moisture) faces limitations in soil observations: the sparseness and very limited horizontal representativeness of in situ observations and the assumptions and resulting (potential) systematic errors inherent in satellite retrievals of the land state despite progress in new instruments. However, analysis increments in the lower atmosphere can provide information on probable errors in land surface fields within a frequently updating NWP system. The MCLDA technique described here does not use in situ or remotely sensed soil observations or full DA covariances, but instead relates near-surface atmospheric analysis increments to soil/snow analysis increments within an overall hourly

cycled data assimilation and forecast system. Its soil increments are affected by all available atmospheric measurements (including soundings, aircraft, satellites, and 2-m screen-level data), while soil increments in ECMWF and UKMO are affected primarily by 2-m measurements and soil-related satellite data. As cited earlier, James and Benjamin (2017) showed a clear improvement in 2-m temperature/moisture forecasts especially in daytime from aircraft and other upper-air observations.

Varying levels of sophistication are possible for coupling land surface and atmospheric data assimilation, ranging from WCDA (in which land surface and atmospheric analyses are carried out separately) to SCDA (in which land surface and atmospheric variables are updated in a unified DA system, with two-way coupling and cross-variable covariances). The MCLDA method is an intermediate approach, taking advantage of the inherent tight coupling between soil/snow evolution and near-surface atmospheric behavior in an NWP system with a continually cycled land surface state. The MCLDA is one component of the larger set of Earth system coupling used in NOAA’s rapidly updating RAP and HRRR models (B16; D22; see Table 3 here).

The MCLDA described here is applied in the vertical to soil and snow temperatures and volumetric soil moisture, and also features a horizontal update to the extent of snow (and ice) cover, with both building and trimming based on satellite-derived daily snow and ice analyses. The MCLDA is applied subject to a number of constraints intended to avoid unrealistic land surface evolution. The land surface fields in the RAP and HRRR models are allowed to evolve via continuous

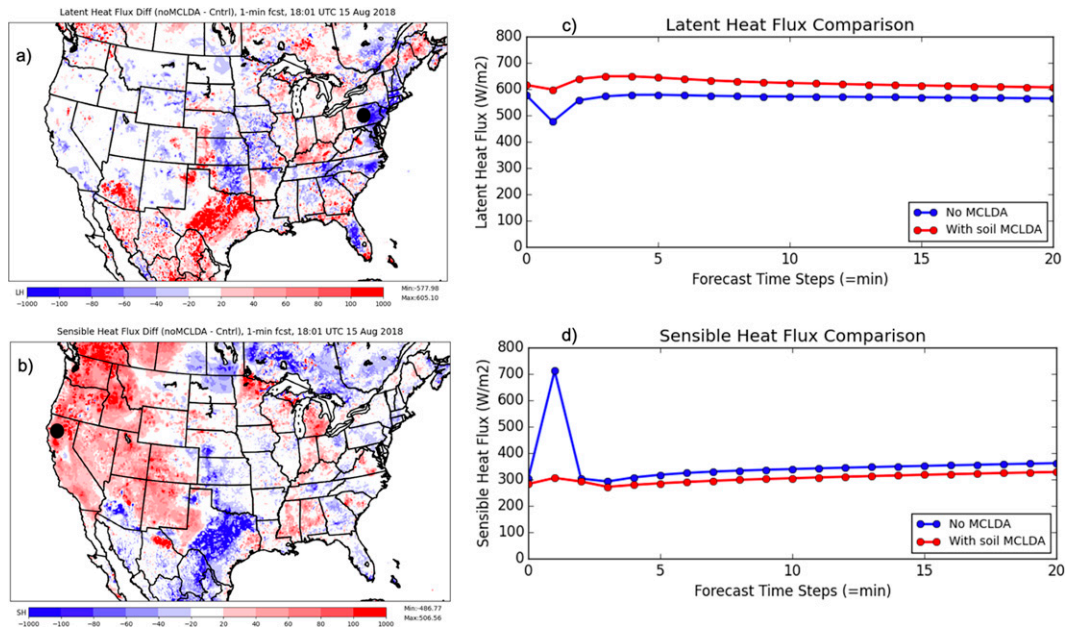


FIG. 13. More flux comparisons for RAP experiments from 15 Aug 2019 at 1801 UTC. Differences (noMCLDA minus control-MCLDA) for (a) latent and (b) sensible heat flux. (c) Latent heat flux time series for each time step comparison out to 20 min for MCLDA and noMCLDA experiments for a point in central PA [black dot in (a)]. (d) Similarly, sensible heat flux time series (from 1800 to 1820 UTC) are shown for the same two experiments for a point in northern California [black dot in (b)].

cycling driven by hourly assimilation applied from the observations shown in Table 4, with the MCLDA approach also applied. The land surface fields for these models have been evolving for many years via the model forecasts themselves in combination with hourly data assimilation and MCLDA. First, an earlier version of the MCLDA method was introduced in the late 1990s on a coarser horizontal scale over CONUS in the Rapid Update Cycle (Benjamin et al. 2004), then in 2011 this evolved land surface state was grafted into the RAP, and since 2012, 3-km land surface variables initialized from the 13-km RAP has been evolving independently in the HRRR. The MCLDA approach has been critical for avoiding any significant drift in soil temperature and moisture evolution over more than two decades on 13- and 3-km resolutions.

In this paper, we demonstrate short-range forecast improvements coming from the application of MCLDA within the hourly 13-km RAP system (B16) compared to an experiment without any land DA. Lower atmosphere observations (both 2-m and rawinsonde-based temperature and humidity) are significantly improved for 6–12-h forecasts and sometimes out to 24 h when MCLDA is applied, most notably during winter when errors in predicting location and amount of snowfall can substantially affect modeled surface properties. The daily snow and ice update based on IMS snow data leads to a more accurate spatial distribution of snow cover, important for predicting the evolution of the planetary boundary layer. Dawson et al. (2016) showed an improved snow evolution from RAP (using MCLDA) versus other NCEP models. The moderately coupled DA described in this paper within the full atmosphere-soil-

snow state enables an initialization of the full atmosphere-soil-snow state and thus avoids initial shock to surface-energy-balance via ensuring accurate fluxes across atmospheric/land (and snow) interface especially in initial forecast hours.

Overall, in this paper, we show the impact of coupled land-snow data assimilation on short-range forecasts from the hourly updated NOAA Rapid Refresh assimilation/modeling system (B16). A coupled data assimilation is important for applications of the short-range rapidly updating NWP, including severe weather/convection, aviation, clouds, energy, precipitation, and extreme cold conditions in winter. Erroneous surface fluxes from strong nonequilibrium land-atmosphere contrasts in the first few timesteps of the model can lead to short-range forecast error for these applications.

Upcoming studies will show comparisons for RAP/HRRR using MCLDA with in situ soil observations [similar to those by Santanello et al. (2019) and Carrera et al. (2019)] and also with PBL surface-energy flux observations. A strongly coupled DA will be developed to initialize the soil, snow, and atmosphere simultaneously. We plan to test the 36-member 3-km HRRR data assimilation system (HRRRDAS; D22) ensemble to evaluate prognostic land-atmosphere vertical covariances, as shown by Lin and Pu (2020), to improve over the MCLDA technique described here. The application of a carefully designed soil parameter perturbation approach will likely be essential for improving ensemble data assimilation and prediction [as demonstrated by Jankov et al. (2017) and refined by Draper (2021)]. Assimilation of microwave indicators of soil moisture (SMAP, SMOS, ASCAT) will be added following effective techniques

described by de Rosnay et al. (2013), Muñoz-Sabater et al. (2019), Bélair and Boone (2020), and others. This work will be conducted under the coupled data assimilation effort for the NOAA Unified Forecast System (UFS).

Acknowledgments. Our manuscript was significantly improved through reviews by and discussions with Jean-François Mahfouf (Météo-France), Stéphane Bélair (ECCC), Clara Draper (NOAA PSL), and Xia Sun (NOAA GSL). We are grateful also for helpful suggestions from two anonymous reviewers.

Data availability statement. HRRR data for all versions (starting in 2014), including soil temperature, soil moisture, and snow water equivalent fields, are now publicly available via archives hosted by Amazon Web Services (<https://registry.opendata.aws/noaa-hrrr-pds/>) and Google Cloud Platform (<https://console.cloud.google.com/marketplace/product/noaa-public/hrrr?project=python-232920&pli=1>). Real-time hourly forecasts are available from the NOAA National Centers for Environmental Prediction (NCEP) Central Operations (NCO) (<https://nomads.ncep.noaa.gov/pub/data/nccf/com/hrrr/prod/>).

REFERENCES

- Aires, F. C., F. Prigent, C. Bernardo, R. Jiménez, P. Saunders, and P. Brunel, 2011: A tool to estimate land-surface emissivities at microwave frequencies (TELSEM) for use in numerical weather prediction. *Quart. J. Roy. Meteor. Soc.*, **137**, 690–699, <https://doi.org/10.1002/qj.803>.
- Balsamo, G., and J.-F. Mahfouf, 2020: Les schémas de surface continentale pour le suivi et la prévision du système Terre au CEPMMT. *Meteorologie*, **108**, 77–81.
- Bélair, S., and A. Boone, 2020: La représentation des surface continentales pour la prévision numérique du temps. *Meteorologie*, **108**, 59–66, <https://doi.org/10.37053/lameteorologie-2020-0017>.
- Benjamin, S. G., and Coauthors, 2004: An hourly assimilation/forecast cycle: The RUC. *Mon. Wea. Rev.*, **132**, 495–518, [https://doi.org/10.1175/1520-0493\(2004\)132%3C0495:AHACTR%3E2.0.CO;2](https://doi.org/10.1175/1520-0493(2004)132%3C0495:AHACTR%3E2.0.CO;2).
- , B. D. Jamison, W. R. Moninger, S. R. Sahn, B. E. Schwartz, and T. W. Schlatter, 2010: Relative short-range forecast impact from aircraft, profiler, radiosonde, VAD, GPS-PW, METAR, and mesonet observations via the RUC hourly assimilation cycle. *Mon. Wea. Rev.*, **138**, 1319–1343, <https://doi.org/10.1175/2009MWR3097.1>.
- , and Coauthors, 2016: A North American hourly assimilation and model forecast cycle: The Rapid Refresh. *Mon. Wea. Rev.*, **144**, 1669–1694, <https://doi.org/10.1175/MWR-D-15-0242.1>.
- , J. M. Brown, G. Brunet, P. Lynch, K. Saito, and T. W. Schlatter, 2019: 100 years of progress in forecasting and NWP applications. *A Century of Progress in Atmospheric and Related Sciences: Celebrating the American Meteorological Society Centennial*, Meteor. Monogr., No. 59, Amer. Meteor. Soc., <https://doi.org/10.1175/AMSMONOGRAPHS-D-18-0020.1>.
- , and Coauthors, 2021: Stratiform cloud-hydrometeor assimilation for HRRR and RAP model short-range weather prediction. *Mon. Wea. Rev.*, **149**, 2673–2694, <https://doi.org/10.1175/MWR-D-20-0319.1>.
- Berbery, E. H., K. E. Mitchell, S. G. Benjamin, T. G. Smirnova, R. Hogue, and E. Radeva, 1999: Assessment of land-surface energy budgets from regional and global models. *J. Geophys. Res.*, **104**, 19 329–19 348, <https://doi.org/10.1029/1999JD900128>.
- Bilodeau, B., M. Carrera, A. Russell, X. Wang, and S. Bélair, 2016: Impacts of SMAP data in Environment Canada's Regional Deterministic Prediction System. 2016 *Int. Geoscience and Remote Sensing Symp.*, Beijing, China, Institute of Electrical and Electronics Engineers, 5233–5236, <https://doi.org/10.1109/IGARSS.2016.7730363>.
- Carrera, M. L., B. Bilodeau, S. Bélair, M. Abrahamowicz, A. Russell, and X. Wang, 2019: Assimilation of passive L-band microwave brightness temperatures in the Canadian land data assimilation system: Impacts on short-range warm season numerical weather prediction. *J. Hydrometeorol.*, **20**, 1053–1079, <https://doi.org/10.1175/JHM-D-18-0133.1>.
- Dawson, N., P. Broxton, X. Zeng, M. Barlage, and P. Holbrook, 2016: An evaluation of snow initializations in NCEP global and regional forecasting models. *J. Hydrometeorol.*, **17**, 1885–1901, <https://doi.org/10.1175/JHM-D-15-0227.1>.
- de Rosnay, P., M. Drusch, D. Vasiljevic, G. Balsamo, C. Albergel, and L. Isaksen, 2013: A simplified extended Kalman filter for the global operational soil moisture analysis at ECMWF. *Quart. J. Roy. Meteor. Soc.*, **139**, 1199–1213, <https://doi.org/10.1002/qj.2023>.
- , G. Balsamo, C. Albergel, J. Muñoz-Sabater, and L. Isaksen, 2014: Initialisation of land surface variables for numerical weather prediction. *Surv. Geophys.*, **35**, 607–621, <https://doi.org/10.1007/s10712-012-9207-x>.
- Dharsni, I., K. J. Bovis, B. Macpherson, and C. P. Jones, 2011: Operational assimilation of ASCAT surface soil wetness at the Met Office. *Hydrol. Earth Syst. Sci.*, **15**, 2729–2746, <https://doi.org/10.5194/hess-15-2729-2011>.
- Dowell, D. C., and Coauthors, 2022: The High-Resolution Rapid Refresh (HRRR): An hourly updating convection-allowing forecast model. Part I: Motivation and system description. *Wea. Forecasting*, <https://doi.org/10.1175/WAF-D-21-0151.1>, in press.
- Draper, C. S., 2021: Accounting for land model error in numerical weather prediction ensemble systems: Toward ensemble-based coupled land/atmosphere data assimilation. *J. Hydrometeorol.*, **22**, 2089–2104, <https://doi.org/10.1175/JHM-D-21-0016.1>.
- , J.-F. Mahfouf, and J. P. Walker, 2011: Root zone soil moisture from the assimilation of screen-level variables and remotely sensed soil moisture. *J. Geophys. Res.*, **116**, D02127, <https://doi.org/10.1029/2010JD013829>.
- Duerinckx, A., R. Hamdi, A. Deckmyn, A. Djebbar, J.-F. Mahfouf, and P. Termonia, 2017: Combining an EKF soil analysis with a 3D-Var upper-air assimilation in a limited-area NWP model. *Quart. J. Roy. Meteor. Soc.*, **143**, 2999–3013, <https://doi.org/10.1002/qj.3141>.
- Dy, C. Y., and J. C.-H. Fung, 2016: Updated global soil map for the Weather Research and Forecasting model and soil moisture initialization for the Noah land surface model. *J. Geophys. Res. Atmos.*, **121**, 8777–8800, <https://doi.org/10.1002/2015JD024558>.
- Ek, M. B., K. E. Mitchell, Y. Lin, E. Rogers, P. Grunmann, V. Koren, G. Gayno, and J. D. Tarpley, 2003: Implementation of Noah land surface model advances in the National Centers for Environmental Prediction operational mesoscale Eta model. *J. Geophys. Res.*, **108**, 8851, <https://doi.org/10.1029/2002JD003296>.
- Fovell, R. G., and A. Gallagher, 2020: Boundary layer and surface verification of the high-resolution Rapid Refresh, version 3.

- Wea. Forecasting*, **35**, 2255–2278, <https://doi.org/10.1175/WAF-D-20-0101.1>.
- Giard, D., and E. Bazile, 2000: Implementation of a new assimilation scheme for soil and surface variables in a global NWP model. *Mon. Wea. Rev.*, **128**, 997–1015, [https://doi.org/10.1175/1520-0493\(2000\)128<0997:IOANAS>2.0.CO;2](https://doi.org/10.1175/1520-0493(2000)128<0997:IOANAS>2.0.CO;2).
- Gomez, B., C. L. Charlton-Pérez, H. Lewis, and B. Candy, 2020: The Met Office operational soil moisture analysis system. *Remote Sens.*, **12**, 36901, <https://doi.org/10.3390/rs12223691>.
- He, S., T. G. Smirnova, and S. G. Benjamin, 2021: Single-column validation of a snow subgrid parameterization in the Rapid Update Cycle Land-Surface Model (RUC LSM). *Water Resour. Res.*, **57**, e2021WR029955, <https://doi.org/10.1029/2021WR029955>.
- Helfrich, S. R., D. McNamara, B. H. Ramsay, T. Baldwin, and T. Kasheta, 2007: Enhancements to, and forthcoming developments in the Interactive Multisensor Snow and Ice Mapping System (IMS). *Hydrol. Processes*, **21**, 1576–1586, <https://doi.org/10.1002/hyp.6720>.
- Hirahara, Y., P. de Rosnay, and G. Arduini, 2020: Evaluation of a microwave emissivity module for snow covered area with CMEM in the ECMWF Integrated Forecasting System. *Remote Sens.*, **12**, 2946, <https://doi.org/10.3390/rs12182946>.
- Hu, M., S. G. Benjamin, T. T. Ladwig, D. C. Dowell, S. S. Weygandt, C. R. Alexander, and J. S. Whitaker, 2017: GSI three-dimensional ensemble-variational hybrid data assimilation using a global ensemble for the regional Rapid Refresh model. *Mon. Wea. Rev.*, **145**, 4205–4225, <https://doi.org/10.1175/MWR-D-16-0418.1>.
- Huffman, G. J., and Coauthors, 2007: The TRMM Multisatellite Precipitation Analysis (TMPA): Quasi-global, multiyear, combined-sensor precipitation estimates at fine scale. *J. Hydrometeorol.*, **8**, 38–55, <https://doi.org/10.1175/JHM560.1>.
- , and Coauthors, 2019: NASA Global Precipitation Measurement (GPM) Integrated Multi-satellite Retrievals for GPM (IMERG) Algorithm Theoretical Basis Doc., version 06, 32 pp., https://pmm.nasa.gov/sites/default/files/document_files/IMERG_ATBD_V06.pdf.
- James, E. P., and S. G. Benjamin, 2017: Observation system experiments with the hourly updating Rapid Refresh model using GSI hybrid ensemble-variational data assimilation. *Mon. Wea. Rev.*, **145**, 2897–2918, <https://doi.org/10.1175/MWR-D-16-0398.1>.
- , and Coauthors, 2022: The High-Resolution Rapid Refresh (HRRR): An hourly updating convection permitting forecast model. Part II: Forecast performance. *Wea. Forecasting*, <https://doi.org/10.1175/WAF-D-21-0130.1>, in press.
- Jankov, I., and Coauthors, 2017: A performance comparison between multiphysics and stochastic approaches within a North American RAP ensemble. *Mon. Wea. Rev.*, **145**, 1161–1179, <https://doi.org/10.1175/MWR-D-16-0160.1>.
- Klein, S. A., X. Jiang, J. Boyle, S. Malyshev, and S. Xie, 2006: Diagnosis of the summertime warm and dry bias over the U.S. Southern Great Plains in the GFDL climate model using a weather forecasting approach. *Geoph. Res. Lett.*, **33**, L18805, <https://doi.org/10.1029/2006GL027567>.
- Kleist, D. T., D. F. Parrish, J. C. Derber, R. Treadon, W.-S. Wu, and S. Lord, 2009: Introduction of the GSI into the NCEP global data assimilation system. *Wea. Forecasting*, **24**, 1691–1705, <https://doi.org/10.1175/2009WAF2222201.1>.
- Koster, R. D., and Coauthors, 2004: Regions of coupling between soil moisture and precipitation. *Science*, **305**, 1138–1140, <https://doi.org/10.1126/science.1100217>.
- Koukoulou, M., C. S. Schwartz, E. I. Nikolopoulos, and E. N. Anagnostou, 2021: Evaluation of the soil state representation in the NCAR Ensemble analysis system. *J. Hydrol.*, **601**, 126617, <https://doi.org/10.1016/j.jhydrol.2021.126617>.
- Krinner, G., and Coauthors, 2018: ESM-SnowMIP: Assessing snow models and quantifying snow-related climate feedbacks. *Geosci. Model Dev.*, **11**, 5027–5049, <https://doi.org/10.5194/gmd-11-5027-2018>.
- Kumar, S. V., R. Reichle, C. Peters-Lidard, R. Koster, X. Zhan, W. Crow, J. Eylander, and P. Houser, 2008: A land surface data assimilation framework using the land information system: Description and applications. *Adv. Water Resour.*, **31**, 1419–1432, <https://doi.org/10.1016/j.advwatres.2008.01.013>.
- Lee, T. R., M. Buban, D. D. Turner, T. P. Meyers, and C. B. Baker, 2019: Evaluation of the High-Resolution Rapid Refresh (HRRR) model using near-surface meteorological and flux observations from northern Alabama. *Wea. Forecasting*, **34**, 635–663, <https://doi.org/10.1175/WAF-D-18-0184.1>.
- Lin, L.-F., and Z. Pu, 2018: Characteristics of background error covariance of soil moisture and atmospheric states in strongly coupled land–atmosphere data assimilation. *J. Appl. Meteor. Climatol.*, **57**, 2507–2529, <https://doi.org/10.1175/JAMC-D-18-0050.1>.
- , and —, 2020: Improving near-surface short-range weather forecasts using strongly coupled land–atmosphere data assimilation with GSI-EnKF. *Mon. Wea. Rev.*, **148**, 2863–2888, <https://doi.org/10.1175/MWR-D-19-0370.1>.
- Lynch, P., 2006: *The Emergence of Numerical Weather Prediction: Richardson's Dream*. Cambridge University Press, 279 pp.
- Ma, H.-Y., and Coauthors, 2018: CAUSES: On the role of surface energy budget errors to the warm surface air temperature error over the central United States. *J. Geophys. Res. Atmos.*, **123**, 2888–2909, <https://doi.org/10.1002/2017JD027194>.
- Mahfouf, J.-F., 1991: Analysis of soil moisture from near-surface parameters: A feasibility study. *J. Appl. Meteor.*, **30**, 506–526, [https://doi.org/10.1175/1520-0450\(1991\)030<1534:AOSMFN>2.0.CO;2](https://doi.org/10.1175/1520-0450(1991)030<1534:AOSMFN>2.0.CO;2).
- Mahfouf, J. F., 2010: Assimilation of satellite-derived soil moisture from ASCAT in a limited-area NWP model. *Quart. J. Roy. Meteor. Soc.*, **136**, 784–798, <https://doi.org/10.1002/qj.602>.
- Mahfouf, J.-F., K. Bergaoui, C. Draper, F. Bouyssel, F. Taillefer, and L. Taseva, 2009: A comparison of two off-line soil analysis schemes for assimilation of screen level observations. *J. Geophys. Res.*, **114**, D08105, <https://doi.org/10.1029/2008JD011077>.
- Menard, C. B., and Coauthors, 2021: Scientific and human errors in a snow model intercomparison. *Bull. Amer. Meteor. Soc.*, **102**, E62–E79, <https://doi.org/10.1175/BAMS-D-19-0329.1>.
- Mitchell, K. E., and Coauthors, 2004: The multi-institution North American Land Assimilation System (NLDAS): Utilizing multiple GCIIP products and partners in a continental distributed hydrological modeling system. *J. Geophys. Res.*, **109**, D07S90, <https://doi.org/10.1029/2003JD003823>.
- Monteith, J. L., 1973: *Principles of Environmental Physics*. Edward Arnold, 241 pp.
- Morcrette, C. J., and Coauthors, 2018: Introduction to CAUSES: Description of weather and climate models and their near-surface temperature errors in 5-day hindcasts near the Southern Great Plains. *J. Geophys. Res. Atmos.*, **123**, 2655–2683, <https://doi.org/10.1002/2017JD027199>.
- Mulholland, D. P., P. Laloyaux, K. Haines, and M. A. Balmaseda, 2015: Origin and impact of initialization shocks in coupled atmosphere-ocean forecasts. *Mon. Wea. Rev.*, **143**, 4631–4644, <https://doi.org/10.1175/MWR-D-15-0076.1>.

- Muñoz-Sabater, J., H. Lawrence, C. Albergel, P. de Rosnay, L. Isaksen, S. Mecklenburg, Y. Kerr, and M. Drusch, 2019: Assimilation of SMOS brightness temperatures in the ECMWF integrated forecasting system. *Quart. J. Roy. Meteor. Soc.*, **145**, 2524–2548, <https://doi.org/10.1002/qj.3577>.
- National Operational Hydrologic Remote Sensing Center, 2004: Snow Data Assimilation System (SNODAS) data products at NSIDC, version 1 [snow depth]. National Snow and Ice Data Center, accessed 6 December 2020, <https://doi.org/10.7265/N5TB14TC>.
- Olson J. B., and Coauthors, 2019a: Improving wind energy forecasting through numerical weather prediction model development. *Bull. Amer. Meteor. Soc.*, **100**, 2201–2220, <https://doi.org/10.1175/BAMS-D-18-0040.1>.
- Olson, J. B., J. S. Kenyon, W. M. Angevine, J. M. Brown, M. Pagowski, and K. Sušelj, 2019b: A description of the MYNN-EDMF scheme and coupling to other components in WRF-ARW. NOAA Tech. Memo. OAR GSD 61, 37 pp., <https://doi.org/10.25923/n9wm-be49>.
- Penny, S. G., and Coauthors, 2017: Coupled data assimilation for integrated earth system analysis and prediction: Goals, challenges and recommendations. WMO Tech. Rep. WWRP 2017-3, 59 pp., <https://repository.library.noaa.gov/view/noaa/28431>.
- Pullen, S., C. Jones, and G. Rooney, 2011: Using satellite-derived snow cover data to implement a snow analysis in the met office NWP model. *J. Appl. Meteor.*, **50**, 958–973, <https://doi.org/10.1175/2010JAMC2527.1>.
- Randall, D. A., and Coauthors, 2019: 100 years of Earth system model development. *A Century of Progress in Atmospheric and Related Sciences: Celebrating the American Meteorological Society Centennial*, Meteor. Monogr., No. 59, Amer. Meteor. Soc., <https://doi.org/10.1175/AMSMONOGRAPHS-D-18-0018.1>.
- Richardson, L. F., 1922: *Weather Prediction by Numerical Process*. Cambridge University Press, 236 pp.
- Rodriguez-Fernandez, N., P. de Rosnay, C. Albergel, P. Richaume, F. Aires, C. Prigent, and Y. Kerr, 2019: SMOS neural network soil moisture data assimilation in a land surface model and atmospheric impact. *Remote Sens.*, **11**, 1334, <https://doi.org/10.3390/rs11111334>.
- Santanello, J. A., P. Lawston, S. Kumar, and E. Dennis, 2019: Understanding the impacts of soil moisture initial conditions on NWP in the context of land–atmosphere coupling. *J. Hydrometeorol.*, **20**, 793–819, <https://doi.org/10.1175/JHM-D-18-0186.1>.
- Skamarock, W. C., and Coauthors, 2019: A description of the Advanced Research WRF model version 4. NCAR Tech. Note NCAR/TN-556+STR, 148 pp., <https://doi.org/10.5065/1dfh-6p97>.
- Smirnova, T. G., J. M. Brown, and S. G. Benjamin, 1997: Performance of different soil model configurations in simulating ground surface temperature and surface fluxes. *Mon. Wea. Rev.*, **125**, 1870–1884, [https://doi.org/10.1175/1520-0493\(1997\)125<1870:PODSMC>2.0.CO;2](https://doi.org/10.1175/1520-0493(1997)125<1870:PODSMC>2.0.CO;2).
- , —, and D. Kim, 2000: Parameterization of cold-season processes in the MAPS land-surface scheme. *J. Geophys. Res.*, **105**, 4077–4086, <https://doi.org/10.1029/1999JD901047>.
- , —, S. G. Benjamin, and J. S. Kenyon, 2016: Modifications to the Rapid Update Cycle land surface model (RUC LSM) available in the weather Research and forecasting model. *Mon. Wea. Rev.*, **144**, 1851–1865, <https://doi.org/10.1175/MWR-D-15-0198.1>.
- Thompson, G., and T. Eidhammer, 2014: A study of aerosol impacts on clouds and precipitation development in a large winter cyclone. *J. Atmos. Sci.*, **71**, 3636–3658, <https://doi.org/10.1175/JAS-D-13-0305.1>.
- Turner, D. D., J. Hamilton, W. Moninger, M. Smith, B. Strong, R. Pierce, V. Hagerty, K. Holub, and S. G. Benjamin, 2020: A verification approach used in developing the Rapid Refresh and other numerical weather prediction models. *J. Oper. Meteor.*, **8**, 39–53, <https://doi.org/10.15191/nwajom.2020.0803>.
- U.S. National Ice Center, 2008: IMS daily northern hemisphere snow and ice analysis at 1 km, 4 km, and 24 km resolutions, version 1. National Snow and Ice Data Center, accessed 17 November 2020, <https://doi.org/10.7265/N52R3PMC>.
- Viterbo, P., and A. C. M. Beljaars, 1995: An improved land surface parameterization scheme in the ECMWF model and its validation. *J. Climate*, **8**, 2716–2748, [https://doi.org/10.1175/1520-0442\(1995\)008<2716:AILSPS>2.0.CO;2](https://doi.org/10.1175/1520-0442(1995)008<2716:AILSPS>2.0.CO;2).
- Weygandt, S. S., S. G. Benjamin, C. R. Alexander, T. G. Smirnova, M. Hu, and E. P. James, 2022: Radar reflectivity-based model initialization using specified latent heating (Radar-LHI) within a diabatic digital filter or preforecast integration. *Wea. Forecasting*, <https://doi.org/10.1175/WAF-D-21-0142.1>, in press.
- Xia, Y., and Coauthors, 2021, Preliminary comparison and evaluation of soil moisture simulated in GFSv15 and GFSv16. *35th Conf. Hydrology*, Online, Amer. Meteor. Soc., 218, <https://ams.confex.com/ams/101ANNUAL/meetingapp.cgi/Paper/378593>.
- , J. Meng, H. Wei, R. Yang, F. Yang, D. T. Kleist, and V. Tallapragada, 2020: Application of the GLDAS framework to the next-version Global Forecast System at NCEP. *34th Conf. Hydrology*, Boston, MA, Amer. Meteor. Soc., 5B.4, <https://ams.confex.com/ams/2020Annual/meetingapp.cgi/Paper/363694>.
- Xie, P., and P. A. Arkin, 1996: Analyses of global monthly precipitation using gauge observations, satellite estimates, and numerical model predictions. *J. Climate*, **9**, 840–858, [https://doi.org/10.1175/1520-0442\(1996\)009<0840:AOGMPU>2.0.CO;2](https://doi.org/10.1175/1520-0442(1996)009<0840:AOGMPU>2.0.CO;2).
- , and —, 1997: Global precipitation: A 17-year monthly analysis based on gauge observations, satellite estimates, and numerical model outputs. *Bull. Amer. Meteor. Soc.*, **78**, 2539–2558, [https://doi.org/10.1175/1520-0477\(1997\)078<2539:GPAYMA>2.0.CO;2](https://doi.org/10.1175/1520-0477(1997)078<2539:GPAYMA>2.0.CO;2).